Dynamics of filopodia tip complexes

by
Karen Cheng

DISSERTATION
Submitted in partial satisfaction of the requirements for degree of
DOCTOR OF PHILOSOPHY

in

Biochemistry and Molecular Biology

in the

GRADUATE DIVISION
of the
UNIVERSITY OF CALIFORNIA, SAN FRANCISCO

Approved:

DocuSigned by:
Dyche Mullins
E4FB70A20A7546F...
Dyche Mullins
Chair

DocuSigned by:
Geeta Narlikar
DocuSigned by:
Geeta Narlikar
Sophie Dumont
DocuSigned by:
Daniel Fletcher
DD28103531044C7...
Daniel Fletcher

Committee Members

Acknowledgements

I thank my PI, Dyche Mullins, for his creative vision and enthusiasm for my thesis project through the years. I very much valued our brainstorm sessions that often ended in Dyche reciting a Russian poem from memory. I am also so grateful for his patience in teaching me how to code and do complex image analysis -- the results from this were such a central part of my project.

I thank my qualifying exam committee (Mark von Zastrow, Ron Vale, Wallace Marshall, and Geeta Narlikar) for helping me to shape my project into something ambitious and creative but also practical.

I thank my amazing thesis committee (Geeta Narlikar, Sophie Dumont, and Dan Fletcher) for their mentorship and support, especially near the end of graduate school in which I needed their wisdom the most. Sophie has an uncanny intuition in checking up on me when I need it the most. I greatly benefited from having two brilliant and kind female scientists on my team and I hope to be like them one day.

I thank Kara McKinley for being my unofficial day-to-day mentor and cheerleader in graduate school. I was sad when she didn't join the Mullins lab but then I got the second-best option when she joined the Vale lab next door. I am so grateful that Kara happened to overhear a frustrated conversation between Dyche and me where we were trying to figure out how to do CRISPR and then approach me to generously share her reagents and protocols. We have become good friends and she has supported me through so many challenging times through the years. I couldn't have done it without her compassion, patience, and science and life wisdom.

I thank Sam Lord for teaching me how to use microscopes and always being a reality check on my science. I knew that if my experiment, analysis, and logic passed the Sam test, it was probably okay for everyone else and I always appreciated the honesty in his feedback. Sam has also just been an awesome lab member and always make my science clearer and better.

I am so lucky and grateful to be part of the Tetrad class of 2014. I discovered some of my closest friends through our cohort and they have been a huge support system in getting through graduate school. In particular, I want to thank Ben Barsi-Rhyne and Kelsey Haas. In addition to being my classmates, they were also just the best roommates. I will always think of our Mission apartment fondly. Even though it was sometimes weird and sketchy because, well, it was the Mission, it was always colorful and a constant adventure. It was always reassuring to know that we could go home at the end of a difficult day and vent and support each other. Though we all now live in different places, I still think of us as the original BKK household.

I want to thank my undergraduate advisor, Anthony Bishop, for inspiring me to go to graduate school. He is the best mentor and human being ever and so calm and balanced and GOOD. I was so spoiled to be his student early on in my scientific career and he will forever be the gold standard of mentors to me.

I am also so grateful to my friends outside of graduate school. Having a life outside of lab has been so key in preserving my sanity and feeling balanced. In particular I want to thank my childhood friends, Stephanie and Tiffany. I'm so glad that we have been in the Bay Area together for the last 5 years or so. Tiff – thank you for inviting me to your house after long days in lab, feeding me, and listening to all of my lab stories. I value our friendship so much and am glad that we've gotten even closer through adulthood. Additionally, I want to thank Laurel Mills. We met through a mutual friend at the beginning of graduate school and clicked immediately in

that way of kindred spirits. The fact that our friendship has persisted and deepened independently has meant the world to me. Thank you for listening to my problems, responding to my million texts throughout the day and just being the most loyal, steadfast friend.

I want to thank my family. Thank you for raising me to value education and science, and for giving me a childhood in which I felt the freedom and privilege to pursue a PhD.

Lastly, I want to thank my partner, Damian. The last few years of graduate school have been so much more joyful with you. Thank you for holding my hand through the ups and downs and for supporting me through this journey. You're the best.

Contributions

Chapter 2 is a reprint of a *Molecular Biology of the Cell* article:

Cheng, K.W. and Mullins, R.D. 2020. Initiation and disassembly of filopodia tip complexes containing VASP and lamellipodin. Molecular Biology of the Cell, p. mbcE20040270.

I conceived, designed, performed the experiments and drafted the manuscript under the guidance of R. Dyche Mullins.

Chapter 3 is an annotated tutorial of Matlab code deposited on Github used for the anaylsis of dynamic cell edges:

R. Dyche Mullins and I wrote the Matlab code for image anaylsis of dynamic cell edges described in Chapter 3. I drafted the annotated tutorial that is deposited on the Mullins lab Github. Samuel J. Lord deposited the code and tutorial on Github.

Chapter 4 is unpublished data associated with the published *Molecular Biology of the Cell* article described in Chapter 2. I conceived and designed all of the experiments under the guidance of R. Dyche Mullins. The fish keratocyte experiments were performed in collaboration with Julie Theriot (Stanford and University of Washington) and her graduate student, Andrew Kennard. The unpublished RNAseq data referred to in Figure 4.1A and the materials used in the fish keratocyte experiments were completely the work of Julie Theriot's lab.

Initiation and disassembly of filopodia tip complexes containing VASP and lamellipodin

by Karen W. Cheng

Abstract

The shape of many eukaryotic cells depends on the actin cytoskeleton, and changes in actin assembly dynamics underlie many changes in cell shape. Ena/VASP-family actin polymerases, for example, modulate cell shape by locally accelerating actin filament assembly and slowing filament capping. When concentrated into discrete foci at the leading edge, VASP promotes filopodia assembly, and forms part of a poorly understood molecular complex that remains associated with growing filopodia tips. Here we identify precursors of this filopodia tip complex in migrating B16F1 cells: small leading-edge clusters of the adaptor protein lamellipodin (Lpd) which subsequently recruit VASP and initiate filopodia formation. Dimerization, membrane association, and VASP binding are all required for lamellipodin to incorporate into filopodia tip complexes, and over-expression of monomeric, membrane-targeted lamellipodin mutants disrupts tip complex assembly. Once formed, VASP and lamellipodin-containing tip complexes grow by fusing with each other, but their growth is limited by a size-dependent, dynamic instability. Our results demonstrate that assembly and disassembly dynamics of filopodia tip complexes are determined, in part, by a network of multivalent interactions between Ena/VASP proteins, EVH1 ligands, and actin filaments.

Table of Contents

List of Figures

List of Tables

List of Abbreviations

CD: Cytochalasin D

EVH1 domain: Ena/VASP homology-1 domain

Lpd: Lamellipodin

MRL: Mig-RIAM-lamellipodin

RA: Ras-association

PH: Plekstrin homology

VASP: Vasodilator stimulated phosphoprotein

Chapter 1: Introduction

An orchestra of actin regulators collaborate at the leading edge of eukaryotic cells to build dynamic actin structures required for cell shape changes and motility. Some of these proteins are dedicated to assembling branched actin networks that form broad, sheet-like structures called lamellipodia, whereas others elongate and bundle actin filaments into thin, protrusive structures called filopodia. Together, these proteins form complex interaction networks that regulate the actin cytoskeleton and cell motility.

While we generally have biochemical and genetic insights into the function of these actin regulatory proteins at the level of the individual proteins, we are still trying to understand the complex behaviors that emerge as these molecular building blocks self-assemble into larger structures. A classic example that demonstrates the value in studying biological molecules across all length scales is the hierarchical organization of monomeric actin into filamentous polymers that can then further organize into macroscopic structures such as lamellipodia and filopodia. At each level of structural complexity, new mechanical properties such as force generation and dynamic membrane protrusion emerge, which are largely unpredictable by studying only the constituent parts. In this body of work, I explore how the clustering of specific actin regulators at lamellipodia transforms its activity into a filopodia initiation complex.

Filopodia are thin, finger-like protrusions of the plasma membrane that participate in fundamental cellular processes, including directed migration, substrate adhesion, and cell-cell communication (Mattila and Lappalainen 2008; Blanchoin et al. 2014). Filopodia are defined by morphology rather than function or composition, and growing evidence suggests that different types of filopodia assemble via different mechanisms that employ different sets of actin regulators (Yang and Svitkina 2011; Barzik et al. 2014; Young et al. 2015; Young et al. 2018). One class of filopodia grows from dynamic, lamellipodial actin networks by a process of “convergent elongation”. In this mechanism, the growing barbed ends of several pre-existing actin filaments converge to a point in the plasma membrane where they are held together by a self-assembling filopodial “tip complex” (Lewis and Bridgman 1992; Svitkina et al. 2003;

Mogilner and Rubinstein 2005). The tip complex contains actin polymerases, such as Ena/VASP-family proteins that accelerate filament growth and inhibit filament capping (Breitsprecher et al. 2008; Hansen and Mullins 2010) and are required for the formation of filopodia in several cell types (Kwiatkowski et al. 2007; Damiano-Guercio et al. 2020). The spatial constraint imposed on growing barbed ends of filaments associated with tip complexes causes them to become aligned and subsequently crosslinked by the protein fascin (Vignjevic et al. 2003).

Clustering of VASP tetramers is a key event in tip complex assembly and an important driver of convergent elongation, but the mechanisms underlying this clustering remain obscure. The Ena/VASP Homology-1 (EVH1) domain determines the subcellular localization of VASP by binding to proteins that contain an FPPPP (or less commonly LPPPP) motif, such as zyxin, vinculin, Abi1, RIAM, and lamellipodin (**Figure 1.1a**; Brindle et al. 1996; Niebuhr et al. 1997; Reinhard et al. 1996; Gertler et al. 1996; Prehoda et al. 1999; Ball et al. 2000; Lafuente et al. 2004; Krause et al. 2004). Specifically, VASP molecules lacking an EVH1 domain fail to find the leading edge, and EVH1 ligand sequences artificially targeted to other cellular compartments, such as mitochondria, can deplete VASP from the leading edge (Bear et al. 2000). Although the EVH1 domain drives localization of VASP, it is unclear whether this domain is also responsible for its incorporation into filopodia tip complexes.

Evidence that EVH1 ligands could promote VASP clustering comes from in vitro studies of lamellipodin (Hansen and Mullins 2015), a leading edge protein that contains six FPPPP motifs and forms membrane-associated dimers (**Figure 1.1A**; Chang et al. 2013). In these studies, purified VASP formed dense co-clusters with lamellipodin (Lpd) constructs on actin filaments. Pre-formed clusters of purified lamellipodin also recruited VASP and dramatically increased the processivity of its actin polymerase activity. In motile cells, lamellipodin helps recruit VASP tetramers to the leading edge via interaction of its Ras-binding and Pleckstrin Homology (RAPH) domains with membrane-associated small G-proteins and phospholipids

respectively (Bear et al. 2002; Krause et al. 2004; Hansen and Mullins 2015). An attractive hypothesis is that VASP tetramers form clusters at the leading edge due to multivalent interactions between their four EVH1 domains and the twelve FPPPP motifs in a lamellipodin dimer. Because both VASP and lamellipodin also bind filamentous actin, clustering might be driven by mutual interactions between three critical components: VASP, lamellipodin, and actin (**Figure 1.1B**).

An alternative set of candidates for driving cluster formation are SH3-containing proteins that interact with recognition motifs (based on pxxp sequences) in the proline-rich region of VASP. These interaction partners include IRSp53 (insulin receptor phosphotyrosine 53 kDa substrate), an I-BAR domain-containing protein that localizes to regions of membrane curvature and promotes formation of long filopodial protrusions (Yamagishi et al. 2004; Millard et al. 2005). IRSp53 is a particularly attractive candidate for initiating filopodia tip complexes (Welch and Mullins 2002; Ahmed et al. 2010), not only because it interacts with VASP, but because its I-BAR domain tubulates membranes *in vitro* and localizes to membrane tubules in live cells (Prévost et al. 2015; Disanza et al. 2013). *In vitro*, purified IRSp53 can recruit VASP tetramers to lipid-coated beads, and a Cdc42-activated IRSp53-VASP complex has been proposed to trigger VASP clustering in cells (Lim et al. 2008; Disanza et al. 2013).

To determine whether EVH1 ligands or SH3 domains drive clustering of VASP and initiation of filopodial bundles, we performed high-resolution time-lapse microscopy of fluorescent actin regulators expressed from their endogenous gene loci in migrating B16F1 mouse melanoma cells. We chose B16F1 cells because they are an excellent model system for studying convergent elongation of leading-edge filopodia: during the initial spreading and polarization phase, VASP localizes along the leading-edge lamellipodial actin network of these cells where it continually coalesces into discrete foci, each of which generates a filopodial actin bundle via convergent elongation (Rottner et al. 1999; Svitkina et al. 2003; Mejillano et al. 2004; Korobova and Svitkina 2008).

Our experiments revealed that nascent VASP clusters generally do not contain IRSp53 but rather arise from pre-existing foci of lamellipodin, and that reducing the valency of binding between VASP and lamellipodin disrupts their ability to co-cluster. Additionally, capping actin filaments causes rapid spatial separation of the VASP and lamellipodin components of the filopodia tip complex, indicating that actin barbed ends play a key role in cluster stability. Surprisingly, our experiments also revealed that filopodia tip complexes undergo a spontaneous, size-dependent splitting, which appears to limit their maximum size. Together, our data indicate that filopodia tip complexes are held together by a dynamic network of multivalent interactions between VASP, lamellipodin, and actin barbed ends.

In Chapter 2, I present the main results of my thesis work pertaining to the initiation and disassembly of filopodia tip complexes. Chapter 3 is organized as an in-depth tutorial of the design and execution of the leading-edge kymograph analysis. Chapter 4 summarizes key unpublished and/or negative data pertaining to my thesis work. I conclude and discuss future directions in Chapter 5.

Chapter 2: Initiation and disassembly of filopodia tip complexes containing VASP and lamellipodin.

Leading-edge dynamics of VASP expressed at endogenous levels in B16F1 melanoma cells.

To visualize VASP in live B16F1 cells, we used CRISPR/Cas9 to create a monoclonal cell line expressing VASP-eYFP from the endogenous gene locus (**Figure 2.1A**, **Figure 2.2A**). Our knock-in strategy enabled us to study protein localization and dynamics without overexpression artifacts and to quantitatively compare fluorescence intensities between cells and across experiments. Similar to previous studies (Reinhard et al. 1992; Gertler et al. 1996), we found that during the early stages of cell spreading and migration, VASP-eYFP localized to nascent focal adhesions (**Figure 2.1A**, dashed ellipse) as well as the leading edge of advancing lamellipodia, where it often concentrated into discrete foci (**Figure 2.1A**, arrowheads; **Figure 2.2B**). Compared to B16F1 cells transiently overexpressing GFP-VASP our engineered cells had significantly fewer discrete VASP foci at the leading edge (**Figure 2.2C**). We occasionally captured *de novo* formation of VASP foci in regions of otherwise uniform VASP density (**Figure 2.1B**), and consistent with previous studies (Svitkina et al. 2003), we observed that VASP clusters skate laterally along the leading edge, often fusing with each other to form larger clusters (**Figure 2.1B**). Stable VASP foci were associated with actin bundles that extend back into the lamellipodial network, and the birth of a VASP focus at the leading edge always heralded the appearance of an associated actin bundle (**Figure 2.1C**). Whenever two VASP clusters fused, their associated actin bundles also zippered together --via a short-lived, lambda-shaped intermediate-- to form a single, larger bundle (**Figure 2.1C**). Overall, the fluorescence intensity of leading-edge actin bundles correlates with the intensity of their associated VASP clusters, suggesting that VASP clusters play a role in creating and maintaining their structure (**Figure 2.1D**). Some VASP-associated actin bundles form filopodia that protrude several microns beyond the leading edge, while others barely dent the membrane surface. The shorter protrusions are often called ‘microspikes’ to distinguish them from longer filopodia (Yang and

Svitkina 2011), but we observed occasional interconversion between these structures and so, consistent with Svitkina et al. (2003), we refer to them collectively as 'filopodial actin bundles'.

To more easily track the creation and evolution of VASP-eYFP clusters across the entire leading edge of spreading and crawling cells, we created automated image analysis tools using MATLAB. Briefly, we used VASP-eYFP fluorescence to find the cell edge in every frame of a time-lapse image sequence (**Figure 2.1E**, left panel), and then --based on membrane morphology and dynamics-- identified leading-edge lamellipodia for further analysis **(Figure 2.1E**, middle panel). For each frame we mapped VASP-eYFP intensity along the cell edge onto a vertical line to create a space-time plot, or kymograph (**Figure 2.1E**, right panel). Unlike kymographs that analyze a fixed region of space, these adaptive kymographs follow the advancing and retracting cell edge and simplify analysis of VASP cluster dynamics by: (1) removing membrane movement; (2) reducing the number of spatial dimensions; and (3) mapping time onto space, enabling us to rapidly identify key events in the life cycle of VASP clusters across many cells. These key events include the birth of nascent clusters; lateral skating of mature clusters; and fusion of colliding clusters.

Lamellipodin is a stoichiometric component of leading-edge VASP foci.

Until now the earliest observable event in filopodial bundle formation has been the formation of leading-edge VASP clusters, so we aimed to identify additional molecules that might initiate and/or stabilize VASP clusters. Multivalent EVH1-binding proteins including Mig10, RIAM, and lamellipodin (collectively, the MRL family of proteins) associate with VASP in leading-edge lamellipodia, but previous studies have disagreed about the association of MRL proteins with VASP foci. Krause et al. (2004) initially observed lamellipodin at the tips of filopodial protrusions and co-localized with Mena and VASP foci at the leading edge, while Disanza et al. (2013) claimed that MRL proteins do not localize into discrete foci at filopodia initiation sites.

To settle the question of whether MRL-family proteins interact with VASP in leading edge clusters and form part of the filopodial tip complex, we created a double CRISPR knock-in B16F1 cell line expressing both VASP-eYFP and a fluorescent lamellipodin-tdTomato fusion protein from their endogenous loci (**Figure 2.3A**). Consistent with the original report of Krause et al. (2004), we found that Lpd-tdTomato localizes along leading-edge lamellipodia and concentrates with VASP at the tips of filopodia. More significantly, all leading-edge VASP foci also contain lamellipodin as a stoichiometric component (**Figure 2.3A**, arrowheads). That is, the ratio of time-averaged, integrated intensities of VASP and Lpd within leading-edge foci was approximately constant (R^2= 0.79) across 58 stable foci observed in ten cells over 4 separate experiments (**Figure 2.3C**, black circles). In contrast, the fluorescence intensities of Lpd and VASP measured along the entire leading edge were much less correlated (**Figure 2.4A**). These results reveal that, even though lamellipodin and VASP are not present at a constant ratio across the entire leading edge, they aggregate with a fixed stoichiometry in stable VASP foci.

IRSp53 does not stably interact with VASP in leading-edge foci.

Disanza et al. (2013) proposed that IRSp53, a dimeric I-BAR domain-containing protein associated with the plasma membrane, binds VASP tetramers and induces them to form stable clusters. Other studies, however, suggest that the connection between VASP and IRSp53 may be less direct (Nakagawa et al. 2003; Sudhaharan et al. 2019). Therefore, to determine whether IRSp53 is present in the early stages of VASP cluster formation, we used CRISPR/Cas9 to create a double knock-in B16F1 cell line, expressing both IRSp53-tdTomato and VASP-eYFP from their endogenous loci (**Figure 2.3B**). We confirmed that the localization of our fluorescent IRSp53 derivative matched that of the endogenous protein using immunofluorescence (**Figure 2.5A**; **Figure 2.5B**). In both live and fixed cells IRSp53-tdTomato was concentrated in patches along the plasma membrane, and often enriched in the shafts of mature filopodia (**Figure 2.3B**, arrowheads). Unlike lamellipodin, however, IRSp53-tdTomato was not a stoichiometric

component of VASP foci, and the correlation between the time-averaged, integrated intensities of VASP and IRSp53 in leading-edge foci (R^2= 0.00014) was not significant (**Figure 2.3C**; **Figure 2.4D**; red squares). Finally, in addition to tagging IRSp53 at the endogenous gene locus, we also transiently overexpressed IRSp53 fused at its N-terminus to mRuby2. Overexpressing this fluorescent fusion protein induced formation of filopodial protrusions containing mRuby2-IRSp53, most of which localized along the shaft of the protrusions but rarely extended out to the tip (**Figure 2.5C**, arrowhead). The majority of VASP-eYFP in these cells remained associated with lamellipodial actin networks, where it formed clusters that contained little or no detectable fluorescent IRSp53. Conversely, the longer protrusions associated with mRuby2-IRSp53 contained little detectable VASP-eYFP at their tips. Together, these localization data indicate that IRSp53 is not a stable or stoichiometric component of leading edge VASP foci.

Dynamics of Lpd and IRSp53 within leading-edge VASP foci.

We next compared the time-dependent changes in the amounts of VASP and its interaction partners, Lpd and IRSp53, within filopodia tip complexes. For this analysis, we computed the cross-correlation between fluorescence intensities of VASP-eYFP and Lpd-tdTomato (or IRSp53-tdTomato) within individual VASP clusters over a time window of 160 seconds. Cross-correlation of VASP and Lpd intensities in leading-edge foci revealed strongly coupled temporal fluctuations. The peak correlation between the two molecules (r = 0.75) occurs at a time lag of 0 seconds, implying that (within the time resolution of our image sequences) fluctuations in the intensity of one molecule do not systematically lead or lag fluctuations in the other (**Figure 2.6A**). In addition, the adaptive kymographs revealed numerous discrete foci of lamellipodin that lack a corresponding accumulation of VASP-eYFP (**Figure 2.6B**, white arrows). These Lpd-only foci were generally smaller, more transient, and exhibited less lateral (skating) movement than foci that contain both VASP and lamellipodin (**Figure 2.6B**, **Figure 2.4B**). Further examination revealed that all nascent VASP foci that we

could detect emerged from these small, pre-existing clusters of lamellipodin (**Figure 2.6B**, white arrowhead). We corroborated these observations by examining the time-lapse movies of the corresponding VASP-lamellipodin clusters, which clearly show that an increased local density of lamellipodin precedes the accumulation of VASP into a detectable focus (**Figure 2.6C**, arrowheads).

We also looked for possible transient interactions between VASP and IRSp53, by asking whether fluctuations in the intensities of these two molecules are also temporally correlated. Maximum cross-correlation between VASP and IRSp53 occurred with a time delay of 8 seconds, which, surprisingly, suggests that VASP might weakly recruit IRSp53 to pre-existing filopodial tip complexes, although the correlation coefficient ($r = 0.093$) was just below the cutoff for statistical significance set by bootstrap analysis ((Zoubir and Iskander 2004); **Figure 2.6D**). Importantly, this fluctuation analysis argues that IRSp53 accumulation at the leading edge is unlikely to drive formation of VASP clusters. Furthermore, comparison of adaptive kymographs displaying VASP-eYFP and IRSp53-tdTomato dynamics along the leading edge of spreading cells revealed no consistent spatial co-localization of the two proteins (**Figure 2.6E).** We also could not detect IRSp53 persistently concentrated in either nascent or stable VASP clusters at the leading edge (Figure **2.6F**). In fact, consistent with our temporal analysis, we occasionally detected accumulation of IRSp53 into pre-existing VASP foci (**Figure 2.6F**, arrow at 24 seconds), suggesting that the VASP molecules occasionally recruit IRSp53 to filopodia tip complexes rather than vise versa.

VASP/Lpd clusters undergo size-dependent splitting events.

Consistent with previous studies of VASP clusters and leading edge microspikes (Svitkina et al. 2003; Oldenbourg et al. 2000), we observed that VASP/Lpd foci grow by both incorporating molecules along the leading edge and by fusing with other foci. Because these filopodia tip complexes remain dynamic and dispersed along the leading edge rather than

accumulating into a single large blob, we hypothesized that, in addition to growth and fusion, tip complexes must also undergo shrinkage and/or fission.

To explore tip complex disassembly, we quantified intensity fluctuations of dynamic VASP/Lpd clusters over time. The simplest assumption --that growth occurs by both the accumulation of individual molecules and the fusion of existing clusters while shrinkage occurs only through loss of individual molecules-- suggests that relative size fluctuations should decrease as clusters grow larger and the ratio of their surface area to volume decreases. By plotting intensity fluctuations as a function of cluster size, however, we found instead that the fluctuations increase nonlinearly with cluster size, implying that VASP/Lpd clusters become more *unstable* as they grow (**Figure 2.7A**). Across all of our experiments, size fluctuations over a 160-second window increased as the 1.75-power of the average cluster size (1.75±0.12; **Figure 2.7A**, inset: log-log plot). A strong inverse relationship between cluster size and stability was apparent no matter how we analyzed the data. For example, using the same data set, we also plotted the distribution of VASP/Lpd intensities of each individual cluster versus its average size (**Figure 2.8A**), and observed the same non-linear increase in vertical scatter with cluster size.

This size-dependent instability imposes an effective limit to the maximum size of filopodia tip complexes, but the physical nature of these size-dependent intensity fluctuations was not clear until we returned to the time-lapse movies and followed the life histories of individual tip complexes. In the largest VASP/Lpd clusters, we identified abrupt and simultaneous drops of both VASP and lamellipodin intensity (**Figure 2.7B**, red arrows) which turn out to reflect dramatic splitting events in which large amounts of VASP and Lpd are simultaneously shed from the cluster (**Figure 2.7C**, yellow arrowhead). In the early stages of tip complex splitting before cluster shrinkage occurs, both VASP and Lpd begin to take on an elongated shape (**Figure 2.7C**, yellow oval dotted line at 20 seconds). As splitting progresses, however, the inward-moving cluster begins to lose lamellipodin, eventually becoming a diffuse

mass of VASP alone (**Figure 2.7C**, 32 seconds). The net result is that the lump of VASP is shed into the cytoplasm, while the lamellipodin is lost by redistribution across the plasma membrane, likely reflecting direct binding of the RAPH domain to phospholipids. Unlike the fusion of tip complexes, which takes place within the leading edge, fission occurs orthogonal to the leading edge, with a chunk of VASP and Lpd moving inward toward the cell body while the rest remains at the leading edge. The portion of the original VASP/Lpd cluster that remains associated with the leading edge exhibits the same dynamics and VASP/Lpd ratio as before the fission event, emphasizing the robustness of the mechanism that maintains the stoichiometry between VASP and lamellipodin in the clusters (**Figure 2.7A-C**; see **Figure 2.8A** for more examples). Additional, static kymograph analysis of splitting events revealed that the detached piece of VASP does not treadmill backward with the retrograde flow of actin, but remains stationary in the laboratory frame of reference as the leading edge moves forward (**Figure 2.7D**). In some examples, VASP shed from a leading edge focus adopted the elongated shape of a nascent focal adhesion, and remained in the same spot for the duration of the movie (**Figure 2.7C**, arrowhead at 32 seconds, **Figure 2.7D**). In total, these data reveal that VASP/Lpd clusters exhibit a form of *dynamic instability*, becoming more unstable as they grow in size.

Actin filaments with free barbed ends are required to form and maintain VASP/Lpd clusters.

In vitro, lamellipodin drives clustering of VASP tetramers on actin filaments (Hansen and Mullins 2015), and in cells the clustering of VASP and lamellipodin occurs only on the outer edge of lamellipodial actin networks, in the dynamic space between the plasma membrane and growing actin filaments. We, therefore, examined whether actin barbed ends might also contribute to cluster formation and/or stability. To test the requirement for barbed ends in VASP/Lpd clustering, we treated B16F1 cells expressing VASP-eYFP and Lpd-tdTomato with Cytochalasin D (CD), a small molecule that rapidly caps free barbed ends. Within 100 seconds

of drug treatment, VASP/Lpd clusters fell apart (**Figure 2.9A**). Cluster dissolution was dramatic and proceeded in two phases. First, all of the leading edge-associated VASP, including the VASP molecules concentrated in filopodial tip complexes, translocated inward toward the cell body, leaving residual, lamellipodin-only clusters behind at the leading edge (**Figure 2.9A**; **Figure 2.9B**). Next, the remaining lamellipodin clusters slowly dissolved as the constituent molecules redistributed laterally across the membrane (**Figure 2.9A**, 200 seconds). We quantified the relative change in lamellipodin clustering immediately following VASP dissociation and 100 seconds later by calculating the standard deviation of its fluorescence intensity along the leading edge normalized to the mean (**Figure 2.9C**; **Figure 2.9D**). Clustering increases the standard deviation while dissolution of clusters into a more uniform distribution causes the standard deviation to fall. The disappearance of lamellipodin clusters suggests that their stability requires VASP and/or actin barbed ends near the membrane.

Lamellipodin requires membrane-targeting and multiple EVH1-binding sequences to incorporate into VASP clusters.

Although lamellipodin is a stoichiometric component of filopodia tip complexes and marks sites where they will form, our cross-correlation data do not reveal whether VASP/Lpd interactions are required to hold the filopodia tip complex together. To investigate the molecular determinants of VASP/Lpd cluster formation, we expressed various lamellipodin mutants and chimeras in our double knock-in B16F1 cell line (**Figure 2.10A; Table 2.2**).

We began by separately overexpressing N- and C-terminal truncation mutants of lamellipodin and asking: (a) whether they were competent to incorporate into endogenous VASP/Lpd clusters, and (b) whether they affected formation of these endogenous clusters (**Figure 2.10B**). The N-terminal region of lamellipodin, comprising the Ras Association and Pleckstrin Homology (RAPH) domain, drives dimerization of the protein and mediates membrane association via interaction with small G-proteins and acidic phospholipids, but lacks

domains that bind VASP. When expressed alone, the RAPH domain localized to the plasma membrane but failed to concentrate at the leading edge, did not incorporate into endogenous VASP/Lpd clusters, and had no effect on cluster formation ('N-term Lpd'; Figure **2.10C)**. This result suggests that lamellipodin does not enter tip complexes via interaction with small G-proteins or acidic phospholipids. We next tested our C-terminal lamellipodin construct, which contains an actin-binding region and six VASP EVH1-binding motifs. Without the RAPH domain, this C-terminal construct failed to strongly localize to the plasma membrane and had no effect on VASP/Lpd cluster formation ('C-term Lpd'; **Figure 2.10D**).

To test whether the inactivity of our C-terminal lamellipodin construct was due to its inability to bind the plasma membrane, we fused C-term Lpd to a membrane-targeting sequence from Lyn_{11} ('Lyn_{11} C-term Lpd'; **Figure 2.10E**). When overexpressed, this monomeric, membrane-associated lamellipodin mutant dramatically disrupted the incorporation of VASP into filopodia tip complexes, resulting in fewer VASP-containing clusters but leaving many small, lamellipodin-only clusters (**Figure 2.10G** vs **Figure 2.10F** control). This construct failed to incorporate into any of the endogenous lamellipodin clusters, suggesting that it acts by sequestering endogenous VASP away from full-length lamellipodin rather than by 'poisoning' the lamellipodin-containing clusters. To test this idea, we mutated all six VASP binding sites ($FPPPP_6 \rightarrow AAPPP_6$) in Lyn_{11} C-term Lpd, to create a monomeric membrane-associated version of lamellipodin incapable of binding VASP. Consistent with a VASP sequestering effect, this mutant construct lost the ability to disrupt endogenous filopodia tip complexes ('VASP-binding mutant'; **Figure 2.10H**).

Finally, we asked what feature of the RAPH domain confers the ability of full-length lamellipodin to incorporate into filopodia tip complexes with VASP. The fact that N-terminal lamellipodin truncations containing the RAPH domain fail to disrupt or incorporate into VASP/Lpd clusters suggested to us that phospholipid and G-protein binding were not involved. However, this leaves open the possibility that dimerization mediated by lamellipodin's RAPH

domain is important for co-clustering by increasing the valency of interactions with VASP. We, therefore, tested whether artificially inducing dimerization of the Lyn_{11} C-term Lpd mutant suffices to revert its dominant negative effect on VASP/Lpd clustering and restore wildtype cluster dynamics. For this experiment, we created a dimeric variant of Lyn_{11} C-term Lpd ('dimerized Lyn_{11} C-term Lpd'; **Figure 2.10l**) by introducing a leucine zipper motif into the N-terminal region. Strikingly, this dimeric, membrane-associated C-terminal truncation mutant did not disrupt filopodia tip complexes like its monomeric counterpart, but was instead concentrated in tip complexes along with wildtype lamellipodin. The effects of dimerization and mutation of EVH1 ligand sequences on the ability of lamellipodin constructs to disrupt or participate in cluster formation argue that VASP/Lpd clusters are held together by multivalent interactions between EVH1 domains of VASP and the FPPPP motifs of lamellipodin and that the valency of these interactions is critical to the stability of the cluster.

Materials and methods

Constructs and reagents

The following primary antibodies and dyes were used for staining: polyclonal rabbit antibody against IRSp53 (4 µg/ml, Atlas Prestige antibodies, HPA023310), monoclonal rabbit antibody against VASP (1:100 dilution, Cell Signaling, #3132), Alexa-647 phalloidin (Thermo Fisher #A22287). Various Lpd constructs were derived from an original plasmid encoding human Lpd^{1-1250}provided by Matthias Krause (King's College, London) and subsequently cloned into a pCMV-SNAP vector.

Cell culture

B16F1 (ATCC-CRL-6323) mouse melanoma cells were cultured in Dulbecco's modified Eagle medium (DMEM) with 4.5 g/mL glucose and supplemented with 10% fetal bovine serum (FBS, Gibco certified, US) and penicillin/streptomycin. Cells were maintained at 37°C and 5% CO_2 and split every 2-3 days. Lipid-based transient transfection was performed using Lipofectamine 3000. For the 6-well plate format, 7.5 µl Lipofectamine 3000 was combined with 1 µg DNA and 5 µl P3000 reagent. The transfection mixture was incubated with 50-70% confluent cells for 8-16 hours and then replaced with fresh media. Cells were assayed or harvested 48 hours later.

Cell line generation

The VASP locus was tagged with eYFP at the C terminus using CRISPR/Cas9-mediated genome engineering in B16F1 cells. The oligonucleotide guide sequences used to cut the targeted genomic sites are listed in Table 1 below. Cas9 and single-guide RNA were expressed using pX330 as previously described (Ran et al. 2013) . Both pX330 and the eYFP-neomycin donor plasmid were a gift of Kara McKinley (UCSF). pX330 and the donor plasmid were co-

transfected into B16F1 cells at 1.25 µg each and selected after 72 hours with 0.8 mg/ml G418 for 2 weeks. Cells that survived antibiotic selection were then analyzed for positive fluorescence (compared to control wildtype B16F1 cells) by fluorescence activated cell sorting (FACS). Fluorescence-positive cells were then individually seeded into 96-well plates and expanded to create stable monoclonal cell lines. Correct fluorescent protein knock-in was verified by PCR/sequencing and fluorescence microscopy. Lpd was sequentially tagged with tdTomato-puromycin at the C terminus using the same strategy as above. eYFP-VASP and tdTomato-Lpd (or tdTomato-IRSp53) double knock-in cell lines were selected using 2 ng/µl puromycin for 5 days and subsequently sorted for monoclonal colonies by FACS.

Sample preparation for microscopy

Glass chambers of varying sizes were cleaned by plasma cleaning for 5 minutes, coated with 50 µg/ml mouse laminin (Sigma #L2020) diluted in PBS, and incubated overnight at 4°C. The day of imaging, laminin-coated glass was rinsed with PBS and replaced with imaging media (Ham's/F12 media + 10% FBS + 50 mM HEPES). B16F1 cells were trypsinized and plated on laminin-coated glass and began to spread within 30 minutes. Cells transfected with SNAP-fusion proteins were labeled with 50 nM Janelia Fluor $SNAP_{646}$-ligand diluted in imaging media for 1 hour upon plating on laminin-coated glass. Janelia Fluor SNAP ligands were a generous gift of Luke Lavis (Janelia Farms). Prior to imaging, the cells were washed with PBS and replaced with fresh imaging media.

Microscopy

Cells were imaged by confocal spinning disk microscopy using a 60x Nikon Plan Apo TIRF (NA 1.49) objective on a Nikon Eclipse microscope fitted with an Andor iXon emCCD camera and controlled by Micromanager 1.4. Cells were maintained at 37°C and 5% CO_2 during imaging using an Okolab stage top incubator and controller. Image processing was performed

using ImageJ/Fiji and custom Matlab code. For experiments in which the barbed ends of actin filaments were blocked using Cytochalasin D (Sigma #C8273), B16F1 cells were first plated on laminin-coated glass as described above. To obtain a baseline before drug addition, we imaged cells for 30 seconds then added 500 nM Cytochalasin D (or DMSO) directly on the microscope stage for acute perturbation. The drug was prepared at 2x concentration in imaging media before addition to cells to achieve a final concentration of 500 nM.

Clustering quantification

VASP clustering at the leading edge was quantified by measuring the background-subtracted fluorescence intensity over an 8-point line width ROI traced along the leading edge in ImageJ/Fiji. The clustering metric was calculated as the standard deviation along the leading edge ROI normalized to the average fluorescence intensity (SD/mean). For paired samples (such as in the cytochalasin D treatments), the drug treated condition was normalized to the control condition.

Chapter 3: Computational anaylsis of dynamic cell edges

We developed two main pieces of custom MATLAB code to aid our analysis of dynamic clusters containing VASP and its binding partners: lamellipodin and IRSp53. First, we wrote cluster tracking analysis to measure the intensity fluctuations of the VASP clusters over a fixed time window. We then wrote edge kymograph analysis code to re-map the dynamic leading edge as a function of time on a space-time plot.

Cluster tracking analysis

To track individual VASP-containing clusters, we developed custom Matlab code to identify and track fluorescent foci through entire time-lapse image sequences. All time-lapse sequences analyzed in this work comprised 40 images of each fluorophore, acquired individually or in pairs at 15 acquisitions/minute. Image acquisition parameters were identical across all experiments. For each frame, we generated an ROI centered on the fluorescent focus and used it to calculate a background-subtracted, integrated intensity. To analyze size fluctuations of individual foci over time we computed the time-averaged intensity and standard deviation for each series. For cross-correlation analysis, we simultaneously imaged fluorescent derivatives of both VASP and either lamellipodin or IRSp53. We computed integrated fluorescence intensities for each time point from the two sets of images to create a pair of intensity vs. time traces. We then subtracted the mean intensity along with the linear and quadratic trends from each data, and used the Matlab xcorr() function to compute a cross-correlation for each pair of traces. We then averaged cross-correlations of multiple foci (>30) from multiple cells (>10) over multiple experiments (>3).

We used a naive bootstrap analysis to set the level of statistical significance for each cross-correlation (Zoubir and Iskander 2004). Briefly, we randomly swapped the data from the two fluorescent channels and calculated the cross-correlation of these unrelated data sets. We calculated average cross-correlations from more than 30 such random permutations for each pair of fluorescent molecules and then calculated the standard deviation at each time lag

position. We marked a minimum criterion for significance on the plots at twice the value of this standard deviation, corresponding to a false positive rate of 0.05.

Edge kymograph analysis

To generate adaptive kymographs to follow fluorescent protein dynamics along a specified leading edge, we developed a Matlab (version compatibility: Matlab 2019a) function that takes in two color time-lapse data sets, uses the marker fluorescence of a designated fluorescence channel to identify the cell edge and, with user input, creates a dynamic region of interest around the cell edge. Tracking and plotting parameters include the following: gaussian blurring used to smoothen images; threshold to find the cell edge; absolute maximum intensity of channel 1 for plot display; absolute maximum intensity of channel 2 for plot display. The moving leading edge is aligned frame-by-frame using autocorrelation. Using this region of interest, the function creates a kymograph for the original channel (VASP) and a second, independent channel (i.e. Lamellipodin or IRSp53).

The following accessory functions in addition to droid5.m (main function) are required in the same file directory:

get_image_names.m

bdy_issues.m

boundary_lines.m

generic_edge2.m

makeline.m

pathfinder2.m

Workflow:

1. Download Matlab code from Github repository: https://github.com/mullinslabUCSF/edge-kymograph

2. Split the two-color time lapse movie into separate channels and save each as an 'image sequence' in separate folders named 'ch1' and 'ch2' for example (**Figure 3.1A**).
3. Create new folders in the same directory called 'results' and 'masked' to store the outputs files.
4. Set the parameter values (blur, threshold, ch1_maxintensity, ch2_maxintensity) in path_param. These values will differ depending on the fluorophore, levels of protein expression, etc and should be checked for each cell that is analyzed.
    1. For reference, the path_param values used to analyze the sample data set is path_param = [5, 0.0049, 4000, 4000].
    2. To determine appropriate threshold and blurring values that yield accurate cell boundary lines, you can separately run the bdy_issues.m function before running the main droid5.m function. This function takes in threshold and blur values and outputs a figure with the boundary lines for the image sequence overlaid. Iterate through different threshold and blur values until the output figure containing overlays of the cell boundary lines yields accurate outlines of the cell perimeter by eye.
4. Once good path_param values are established, run the main function: droid5.m.
5. An interactive figure will pop up with the overlaid boundary lines of the cell. To help the function determine the region of interest, click on the inside and outside of the (1) start point (2) end point (3) midpoint of the boundary lines (**Figure 3.1B**). Then click twice outside of the cell to make a small square (4) for background subtraction for photobleaching calculations.
6. Once the dynamic region of interest is selected with input from the user, droid5 runs and outputs the following figures and saves the kymograph information to the results directory (**Figure 3.1C-F**).

Chapter 4: Unpublished data

The following sets of experiments were performed as a part of my thesis work regarding VASP/lamellipodin clustering but were not included in the final *Molecular Biology of the Cell* publication.

Reconstitution of VASP/Lpd clusters in zebrafish keratocytes

Previously, our lab successfully reconstittued VASP/lamellipodin clusters bound to actin filaments using purified proteins, suggesting that these three core proteins were sufficient to drive clustering in vitro (Hansen and Mullins 2015). On the other end of the spectrum, I had observed robust VASP/Lpd clusters in all the mammalian cell lines (B16F1, HEK293) that I had looked in that made filopodia bundles and expressed VASP and lamellipodin proteins. Inspired by comments by Ron Vale, we wondered whether there was a specific cell line that didn't make filopodia bundles and whether this was dependent on the presence of VASP and/or lamellipodin protein expression and clustering. In other words, did a "blank slate" cell line exist that contained most of the normal actin cytoskeletal machinery but lacked filopodia in which we could cleanly test our VASP/Lpd clustering hypothesis?

Zebrafish keratocyte cells have classically been a model organism to study cell migration and the actin cytoskeleton. Interestingly, fish keratocytes have a broad, fan-like lamellipodia but are not known to make endogenous filopodia bundles. These cells express VASP, which localizes tightly and uniformly to the leading edge and plays a role in lamellipodial smoothness, but the VASP molecules do not coalesce into clusters (Lacayo et al, 2007). Additionally, in conversations with Julie Theriot, an expert in fish keratocyte cell biology, we learned that their preliminary RNAseq data predicted relatively high expression levels of VASP but negligble amounts of lamellipodin (**Figure 4.1A**, unpublished data by Theriot lab). We therefore were excited to test whether exogenous expression of Lpd could induce the clustering of VASP to make filopodia bundles. We collaborated with the Theriot lab and her graduate student Andrew Kennard in the following experiments.

First, we injected embryonic zebrafish keratocytes with human mCherry-lamellipodin (hLpd) and a GFP transgenic marker and imaged migrating cells using spinning disk confocal (data not shown). We observed that a pool of mCherry-hLpd localized to the leading edge of the migrating fish keratocytes but did not form noticeable clusters. Moreover, when we stained the actin cytoskeleton using phalloidin, we also did not observe filopodia bundles. We hypthesized that due to significant protein sequence divergence of human lamellipodin with the zebrafish counterpart (62% similarity), that the endogenous zebrafish VASP may not be able to bind human Lpd. We therefore devised a follow-up experiment in which we co-overexpressed equimolar human VASP and human Lpd in embryonic zebrafish keratocytes using a self-cleaving P2A peptide system (**Figure 4.1B**). Overexpressed hVASP and hLpd localized to the leading edge membrane in a tight even line as expected, but they did not form large clusters with each other nor did they induce noticeable filopodia bundles (**Figure 4.1C**). The actin dynamics of fibroblast-like cells such as B16F1 mouse melanoma differ significantly from the those of fish keratocytes, as they migrate up to 5 times faster than typical human cells. For example, we reasoned that the lamellipodial dendritic network of fish keratocytes could be more entangled and denser, which could impede the skating and clustering dynamics of VASP and lamellipodin. As a final effort, we decided to alter leading edge actin dynamics by acutely adding the actin inhibitors, cytochalasin D and latrunculin B. We and others have shown that capping actin filaments can induce a switch between lamellipodial and filopodia actin architectures (Meijillano et al, 2004). We therefore added 4 nM cytochalasin D to the migrating fish keratoyctes to decrease the density of free barbed ends at the leading edge (**Figure 4.1C**). We observed that the cells stopped actively migrating upon drug addition but there was no noticeable effect on VASP/Lpd clustering. Next, we added 6 uM latrunculin B and again saw that the fish keratocyte cells were less migratory but blocking active actin polymerization also did not have an effect on VASP/Lpd clustering. In conclusion, our effforts to reconstitute VASP/Lpd clustering and filopodia in an orthogonal system such as fish keratocytes could not

recapitulate clustering that we see in mammalian systems. We do not necessarily think this diminishes our identification of VASP and Lpd as key proteins that are clustered to trigger filopodia initiation in many cell types, but these results highlights there is a range of actin dynamic parameters that are also important in defining the specific cell's ability to organize filopodia actin bundles at the leading edge.

Inhibition of actin dynamics and VASP/Lpd clustering

We were inspired by the dramatic dissolution of clusters containing VASP and lamellipodin upon acute capping of barbed ends by cytochalasin D to investigate how other actin inhibitors might affect this process at the leading edge. We first treated B16F1 cells expressing VASP-eYFP and Lpd-tdTomato from their endogenous loci with a potent pharmalogical cocktail called 'JLY' (containing 10 uM Y27632, 8 uM Jasplakinolide, and 5 uM Latrunculin B) which has been reported to freeze actin dynamics (Peng et al, 2011). Upon treatment with the JLY cocktail, cell migration halted and the leading edge became much less dynamic over time (**Figure 4.2A**). Interestingly, clusters containing VASP and lamellipodin gradually dissolved which was reminiscent of the cytochalasin D drug treatment, albeit on a slow time scale (minutes rather than seconds). We reasoned that the JLY cocktail inhibits actin polymerization, depolymerization and retrograde flow but does not affect natural capping of actin filaments by capping protein. Therefore, the dissolution of VASP/Lpd clusters we see in this JLY experiement confirms our observation in the cytochalasin D experiment that free barbed ends are essential for VASP/Lpd clustering in cells.

A longstanding question in the field is whether filopodia actin bundles are initiated from preexisting branched actin filaments nucleated by the Arp2/3 complex or de novo long filaments nucleated by the formin family of actin nucleators (Yang and Svitkina, 2011). To distinguish the source of actin filaments attached to filopodia tip complexes containing VASP and lamellipodin as formin or Arp2/3 generated, we treated B16F1 cells expressing VASP-eYFP and Lpd-

tdTomato with the pan-formin inhibitor SMIFH2. With the caveat that SMIFH2 inhibits all formins and has also been reported to inhibit myosins in vitro at similar concentrations, we found that inhibiting formins had no visible effect on VASP/Lpd clusters and filopodia bundles (**Figure 4.2B**). In particular, we noted that new VASP/Lpd clusters can be initiated even after SMIFH2 is added to the cell and that these filopodia bundles can protrude outward from the cell. This suggests that formins are not required for the initiation of filopodia containing VASP/Lpd clusters at their tips.

Chapter 5: Discussion and future directions

The size, shape, and stability of actin-filled pseudopods depend on the dynamic localization of actin regulators at the plasma membrane (Weiner et al. 2007; Schmeiser and Winkler 2015; Fritz-Laylin et al. 2017). These regulators include VASP and its relatives Mena and Evl, which are weakly processive polymerases that promote rapid growth of actin filaments near the membrane and help construct sheet-like lamellipodia (Lacayo et al. 2007) and finger-like filopodia (Han et al. 2002; Svitkina et al. 2003; Kwiatkowski et al. 2007). To form filopodia, VASP tetramers must be collected into dense clusters, called filopodia tip complexes. By monitoring the leading-edge dynamics of VASP and its binding partners, we discovered a precursor of the filopodia tip complex: a molecular cluster containing the VASP binding partner, lamellipodin (**Figure 5.1**). We also discovered that filopodia tip complexes experience a size-dependent form of dynamic instability.

The role of I-BAR proteins in filopodia assembly.

Similar to previous studies, we find that overexpressing the membrane-associated protein, IRSp53 strongly induces formation of filopodia. Both overexpressed and endogenous IRSp53 localize along the shaft of filopodial protrusions, consistent with the preferential binding of its I-BAR (inverse-Bin-Amphiphysin-Rvs) domain to regions of negative membrane curvature (Yamagishi et al. 2004; Saarikangas et al. 2009). *In vitro*, the I-BAR domain from IRSp53 can tubulate $PI(4,5)P_2$-containing vesicles (Mattila et al. 2007; Prévost et al. 2015), and when overexpressed in cells, it can even drive formation of tubular membrane protrusions that lack filamentous actin altogether (Yang et al. 2009). Although these results illustrate how easily membrane protrusion can be uncoupled from actin filament assembly, IRSp53 has also been shown to interact, via its SH3 domain, with various actin regulators, including VASP, Mena, N-WASP, mDia1, and Eps8 (Krugmann et al. 2001; Ahmed et al. 2010). Based on its interactions with curved membranes, actin regulators, and signaling molecules such as Cdc42, we and others (Welch and Mullins, 2002; Ahmed et al., 2010) suggested that IRSp53 might trigger

filopodium formation by coupling actin assembly to membrane bending. Disanza et al. (2013) further proposed that IRSp53 actually drives formation of filopodial actin bundles by co-clustering with VASP molecules. This attractive idea is generally consistent with the localization IRSp53 to filopodial protrusions, but the strong preference of IRSp53 for curved membranes means it can localize to filopodia and lamellipodia even in Ena/VASP-deficient MV^{D7} cells (Nakagawa et al. 2003). We posed a more stringent test of IRSp53's involvement in VASP clustering by asking whether IRSp53 associates with nascent VASP foci, or whether it forms foci that subsequently recruit VASP. Using fluorescent proteins expressed from the endogenous loci, we found that the coalescence of VASP molecules into foci at the leading edge did not correlate with the presence of IRSp53. Moreover, we observed that VASP foci do not consistently contain detectable amounts of IRSp53 (Figure 2,3). These results fit with recent super-resolution light microscopy studies that found IRSp53 predominantly associated with the lateral edges of filopodia and not consistently enriched at the tip with VASP (Sudhaharan et al. 2019). Our data support the idea that IRSp53 induces protrusion of long filopodia by promoting and stabilizing membrane curvature rather than by clustering VASP tetramers.

The role of EVH1 ligands in VASP localization and clustering.

VASP is recruited to membranes by the interaction of its Ena/VASP Homology 1 (EVH1) domain with proteins that contain FPPPP motifs. This was most clearly demonstrated by Bear et al. (2002), who found that VASP can be displaced from leading edge membranes by removing the EVH1 domain or ectopically expressing FPPPP-containing proteins on intracellular membranes. In addition to lamellipodin, several other proteins with EVH1-binding motifs are found on leading edge membranes. These include Mig10 and RIAM which, together with lamellipodin, define the MRL protein family (Coló et al. 2012).

When we compared the dynamics of endogenous VASP and lamellipodin during filopodia initiation, we found that VASP clusters form on pre-existing foci of lamellipodin. The

small lamellipodin puncta form independently of VASP, but 'ripen' and grow much larger when they begin to accumulate VASP. This observation reveals that small lamellipodin puncta are precursors to larger VASP/lamellipodin clusters that concentrate at the tips of nascent filopodia bundles and raises the question of how small lamellipodin puncta form in the first place. Two possibilities are: (a) lamellipodin can independently form small homo-oligomers, which is supported by a structural study that identified two dimerization motifs at its N-terminal RAPH domain (Chang et al. 2013), or (b) lamellipodin foci mark the position of larger complexes that contain other, as yet unidentified proteins.

Our results provide compelling evidence that interactions between VASP, lamellipodin, and actin barbed ends help hold filopodia tip complexes together. We found, for example, that monomeric, C-terminal Lpd mutants disrupt formation of VASP clusters, a result that could be rescued by simply dimerizing the mutant. We also identified the key features of Lpd that promote VASP clustering: membrane association, dimerization and EVH1-binding. Surprisingly, the N-terminal Ras-association (RA) plekstrin homology (PH) signaling domain of Lpd appears largely dispensable for VASP clustering as we could functionally replace it with a Lyn_{11} membrane tether and a leucine zipper dimerization domain. Based on our results, we propose that the primary function of the RAPH domain is membrane localization and dimerization, rather than clustering per se. This proposal agrees with several studies demonstrating that the PH domain Lpd recruits the protein to the plasma membrane by binding $PI(3,4)P_2$ (Bae 2010, Venkatareddy 2011). Our proposal also fits with a recent structural study of lamellipodin's N-terminal region which suggests that its dimeric RAPH domain has lower affinity for Ras GTPases than individual RA domains found in other proteins, and may make minor contributions to clustering on membranes (Chang et al. 2013).

While multiple lines of evidence indicate that FPPPP-EVH1 interactions are responsible for VASP localization to the leading edge, Dimchev et al. reported that knocking out lamellipodin by CRISPR/Cas9 in B16F1 cells does not significantly change VASP recruitment to lamellipodia

(Dimchev et al. 2019; Bear et al. 2002). This result suggests the existence of redundancy or compensation in the expression of FPPPP-containing proteins. For example, Dimchev et al (2019) also reported that leading-edge localization of a member of the WAVE Regulatory Complex, Abi1, which binds EVH1 domains through an alternate proline motif was increased upon Lpd knockout and may allow it co-cluster with VASP in the absence of lamellipodin (Chen et al. 2014; Dimchev et al. 2019). In addition, lamellipodin is just one member of the MRL family of proteins, which all interact with VASP through FPPPP proline motifs and could potentially replace Lpd's VASP-specific functions at the leading edge.

Disassembly of VASP/Lpd clusters.

VASP/Lpd clusters continuously undergo assembly and disassembly in order to maintain a dynamic distribution along the leading edge. Growth of clusters through gradual accumulation of monomers or abrupt fusion events must be counterbalanced by a disassembly mechanism to prevent the total coalescence of VASP into a few large, static foci at the leading edge. By analyzing VASP cluster size fluctuations, we discovered a disassembly mechanism whereby VASP/Lpd clusters undergo size-dependent splitting events. During splitting, a bolus of VASP detaches from a cluster and moves into the cytoplasm while an equimolar amount of Lpd redistributes evenly back into the plasma membrane. The larger the VASP/Lpd cluster grows, the more unstable it becomes and the instability grows as the approximate square of the cluster size. The fact that these splitting events occur perpendicular to the plasma membrane while fusion events occur parallel to the membrane indicates that splitting is not simply the reverse of fusion, but a separate process with a different underlying molecular mechanism. In addition to maintaining dynamic VASP clusters, splitting might help relocalize VASP tetramers to other parts of the cell. For example, in some cases where nascent focal adhesions are proximal to the leading edge, we observed blobs of VASP splitting from the plasma membrane focus and almost immediately becoming immobilized in the elongated shape of a focal adhesion. As

several focal adhesion proteins (such as vinculin and zyxin) directly bind VASP through the FPPPP-EVH1 interaction module, it is possible that fission of large VASP/Lpd clusters helps deposit VASP directly onto nascent focal adhesions.

In the future, elucidating the molecular and physical mechanisms that drive size-dependent splitting of larger VASP/Lpd clusters will be important. First, structural studies using correlated light and electron microscopy (inspired by work from Tatyana Svitkina) that captured a rare splitting event could give us insights into the structure of the unstable filopodia tip complex during splitting. Because endogenous size-dependent splitting is a rare event, we could induce dissolution of clusters by adding cytochalasin D if it is too challenging to capture an endogenous splitting event. In addition, it would be informative to create a cell line that expresses fluorescent VASP, lamellipodin and actin so that all three molecular components can be reliably quantified and compared across experiments to determine the ratio of VASP:Lpd:actin in a filopodia tip complex. We could test the hypothesis that an “ideal” ratio of VASP:Lpd:actin favors the assembly of the tip complex and actin bundle, whereas deviations from an ideal ratio could induce instability and size-dependent splitting events to occur. Finally, creating a photoactivatable VASP cell line could allow us to track the cellular destination of VASP when it falls off the main cluster during a splitting event. We could specifically test the hypothesis that VASP molecules incorporate into focal adhesions.

In conclusion, we find that VASP clusters assemble at pre-determined sites on the plasma membrane, marked by the presence of its binding partner, lamellipodin. To remain in a cluster, VASP must maintain interactions with both FPPPP-containing ligands *and* free barbed ends of actin filaments. Finally, and most unexpectedly, we find that VASP cluster growth is limited by an intrinsic, size-dependent instability. We propose that the size-dependent instability of VASP clusters reflects the difficulty of coordinating VASP’s interaction with the two binding partners that hold the cluster together: FPPPP-containing proteins and free barbed ends of actin filaments.

Figures and legends

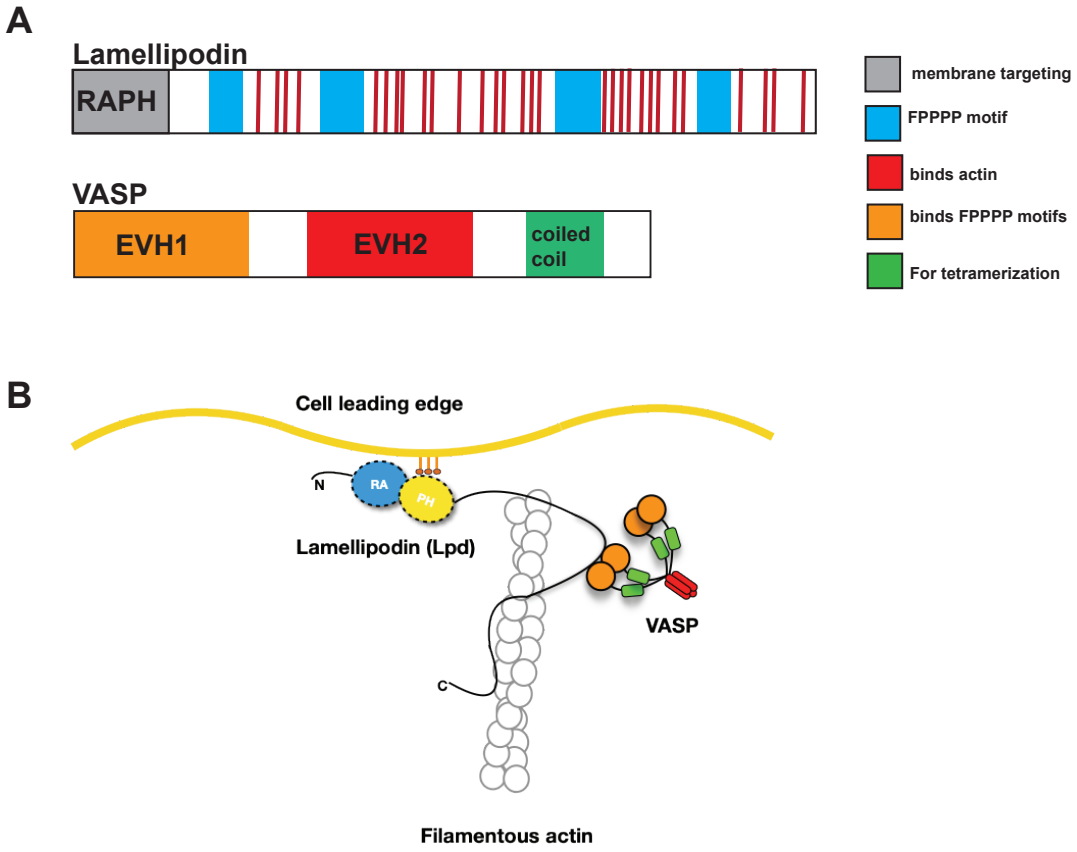

Figure 1.1: Cartoons of the protein structures of VASP and lamellipodin.

(A) Protein domain architectures of lamellipodin (top) and VASP (bottom). Key features of lamellipodin include the RAPH domain which directly binds lipids and small GTPases; 6 F/LPPPP motifs that span four regions; weak C-terminal filamentous actin binding sites. Key features of VASP include the EVH1 domain which binds F/LPPPP domains; EVH2 domain which binds monomeric and filamentous actin; a coiled coil region that mediates tetramerization. (B) Model of interactions between VASP, lamellipodin, and filamentous actin at the plasma membrane in cells.

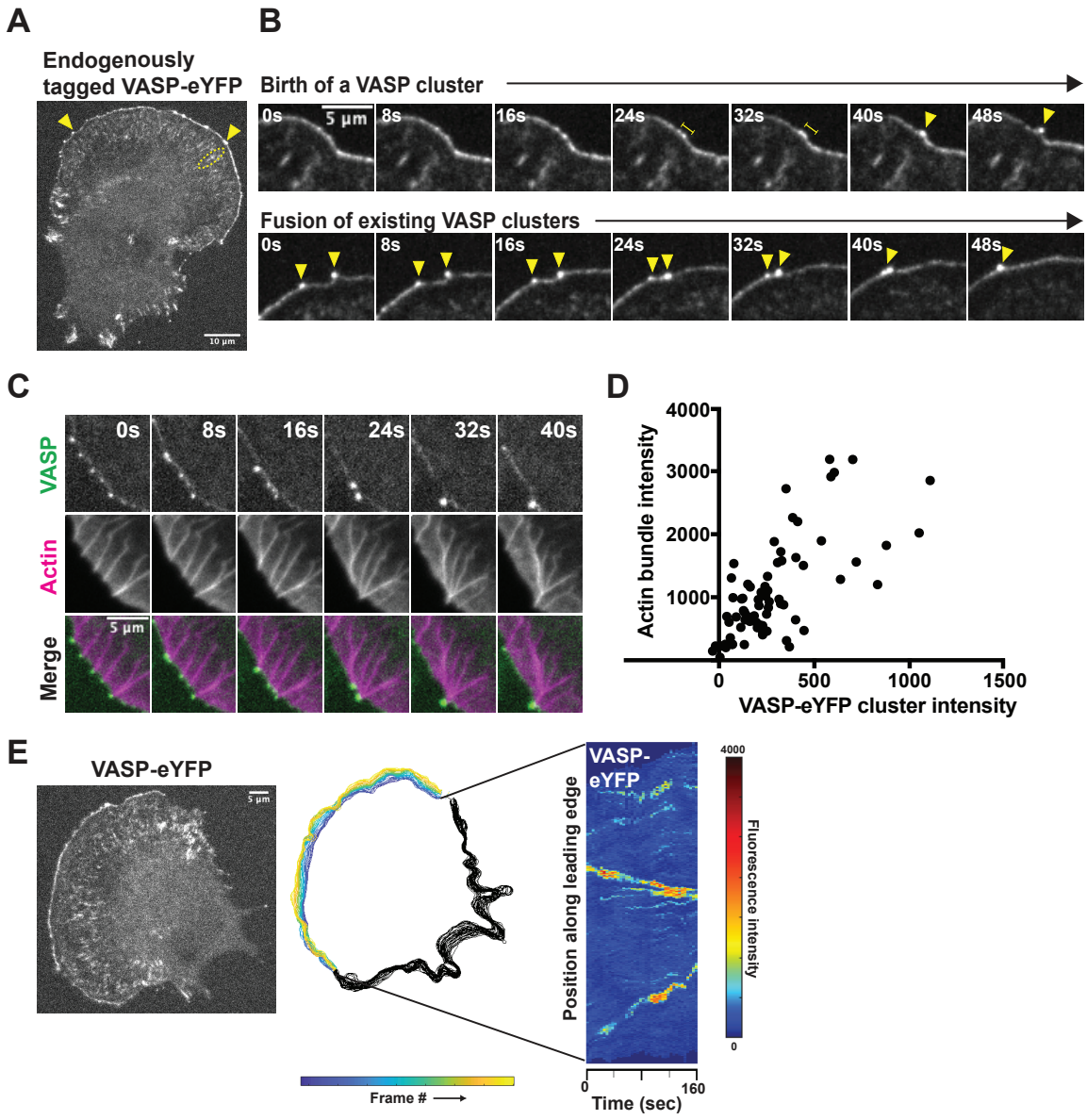

Figure 2.1: Endogenous VASP-eYFP localization and dynamics during B16F1 cell migration.

(A) Representative image of monoclonal, endogenously expressed VASP-eYFP B16F1 cell line generated by CRISPR/Cas9. Yellow arrowheads: VASP clusters; Yellow circle: focal adhesions. (B) Two examples of nascent VASP clusters being born from fluctuations in VASP intensity along the leading edge (top panel) and fusion of existing VASP clusters (bottom panel) by live cell microscopy of the VASP-eYFP B16F1 cell line. Yellow bars: coalescence of VASP-eYFP intensity; yellow arrowheads track VASP-eYFP clusters. (C) Coupled kinetics of VASP-eYFP (green) clustering and $SNAP_{JF646}$-actin bundle (magenta) formation and zippering. (D) Correlation between integrated VASP cluster intensity and underlying actin bundle intensity in 73 foci and 10 cells. (E) Fluorescent image of a representative VASP-eYFP B16F1 cell (left panel) that was used to generate colored outlines of the leading edge position over time (middle

panel). Adaptive kymograph map (right panel) re-maps the leading-edge position to the y-axis and time (40 frames or 160 seconds) on the x-axis to visualize VASP-eYFP foci dynamics. Colormap: blue (low fluorescence intensity) to red (high fluorescence intensity).

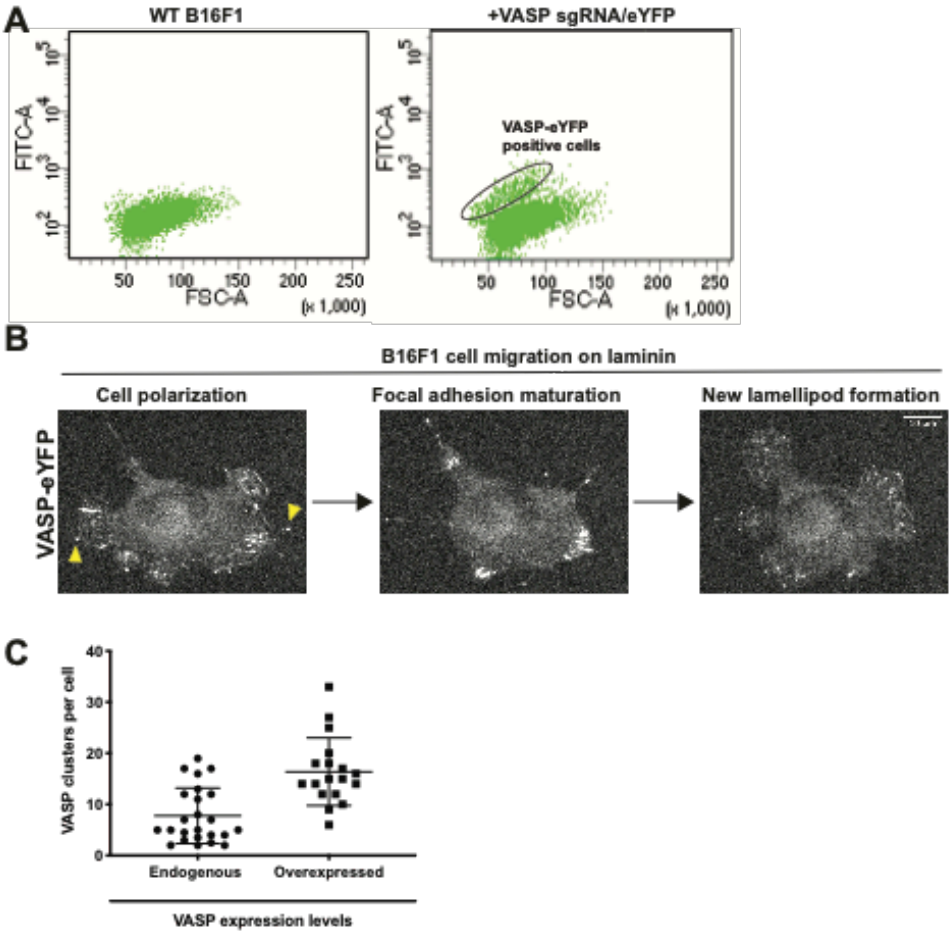

Figure 2.2: Generation of monoclonal VASP-eYFP B16F1 mouse melanoma cell line.

(A) Dot plot from fluorescence activated cell sorting (FACS) of B16F1 cells transfected with Cas9/VASP-specific sgRNA and C-terminal eYFP tag repair template compared to WT B16F1 cells. (B) Endogenously tagged VASP-eYFP B16F1 cells display normal migratory behavior on laminin coated glass. Cell polarization leads to formation of a leading edge with correct VASP localization at lamellipodia, filopodia, and focal adhesions (Yellow arrowheads). Over time, the cell creates mature focal adhesions which is followed by new lamellipod formation and migration in a new direction. (C) The number of VASP clusters per cell in endogenously tagged VASP-eYFP cells or overexpressed GFP-VASP were calculated by counting the number of VASP clusters per 160 second time window using a Z-projection of the movie stack for easy visualization.

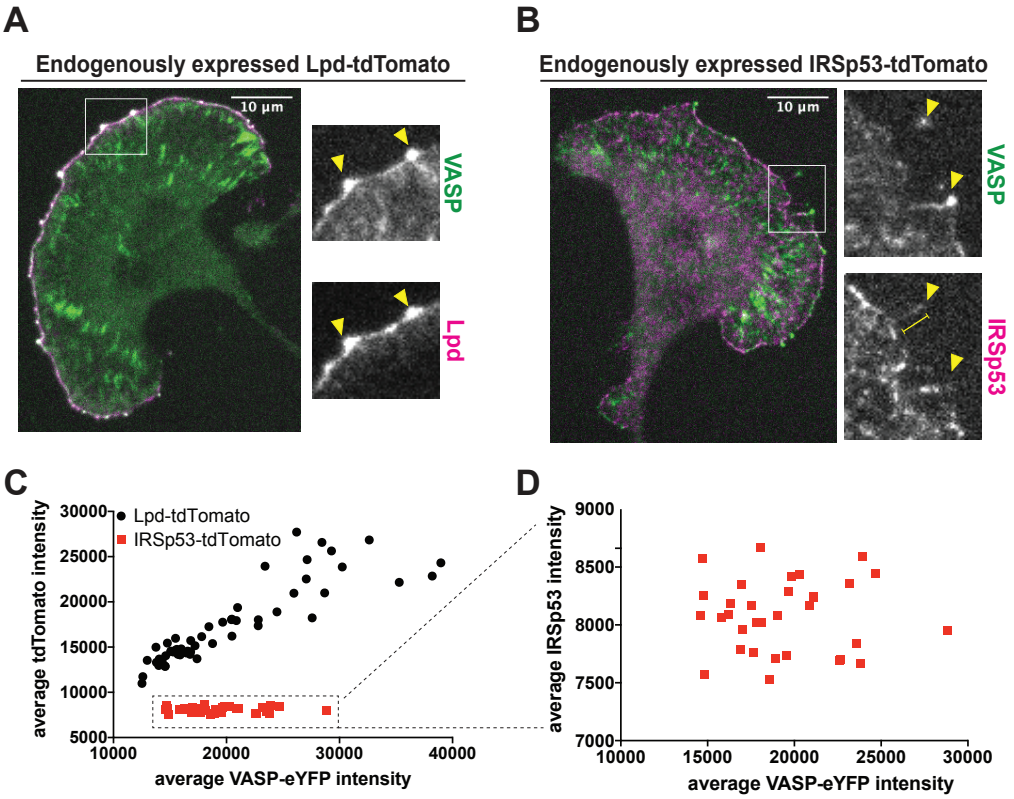

Figure 2.3: Differential localization of the VASP binding partners, lamellipodin (Lpd) and IRSp53, at the leading edge.

(A) Representative image of monoclonal, endogenously expressed VASP-eYFP and Lpd-tdTomato B16F1 cell line shows strong colocalization of the two proteins at VASP foci. Arrowheads: VASP-eYFP foci. (B) Representative image of monoclonal, endogenously expressed VASP-eYFP and Lpd-tdTomato B16F1 cell line shows poor colocalization of the two proteins at VASP foci. Arrowheads: VASP-eYFP foci; yellow bar: filopodia shaft. (C) The time-averaged integrated intensities of VASP-eYFP and Lpd-tdTomato within leading edge foci are tightly correlated (black circles). A plot of average Lpd intensity versus VASP intensity fits a straight line (R^2=0.79). In contrast, the integrated intensities of VASP-eYFP and IRSp53-tdTomato within leading edge foci are not correlated (red squares; R^2=0.00014). (D) Zoomed plot of the VASP-eYFP and IRSp53-tdTomato dataset shows the lack of correlation in their intensities.

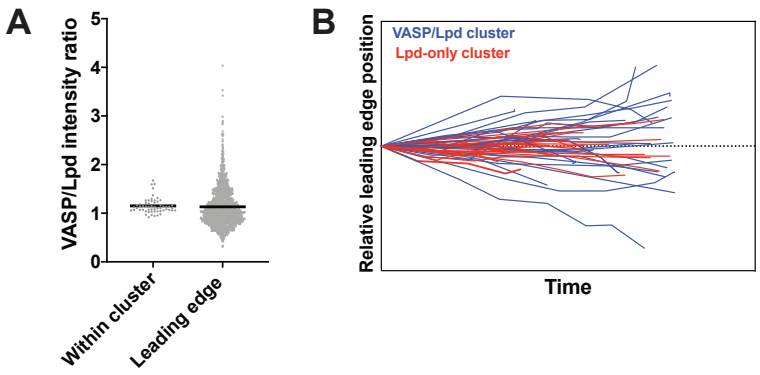

Figure 2.4: Distinct dynamics within VASP/lamellipodin clusters compared to the entire leading-edge.

(A) The ratio of VASP to lamellipodin intensities within clusters were compared to the ratio of VASP to lamellipodin intensities along every point on the leading edge of B16F1 cells. (B) Quantification of lateral skating movement of VASP/Lpd clusters (30 cluster tracks) vs. clusters that only contain Lpd (23 cluster tracks) along the leading edge. The starting position was normalized to begin at the same point for all tracks.

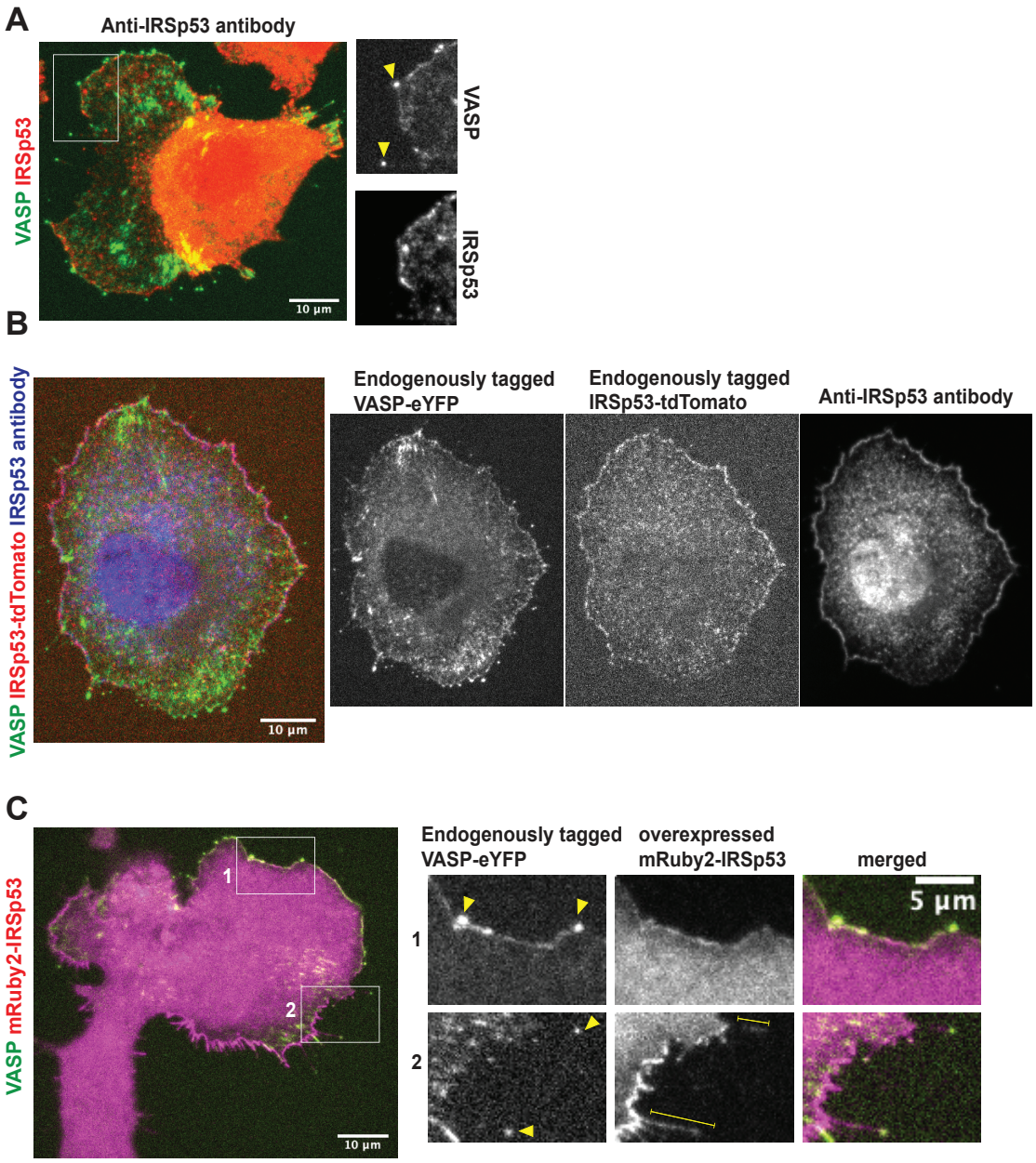

Figure 2.5: Localization of endogenous and overexpressed IRSp53.

(A) Immunofluorescence of endogenous IRSp53 (red) in VASP-eYFP (green) tagged B16F1 cells. Arrowheads: VASP-eYFP foci; yellow bar: filopodia shaft. (B) Verification of double CRISPR knock-in VASP-eYFP/IRSp53-tdTomato B16F1 cells by immunostaining with a polyclonal IRSp53 antibody and secondary Alexa 647 antibody. (C) Localization of overexpressed, N-terminally tagged mRuby2-IRSp53 in the context of the VASP-eYFP B16F1 CRISPR knock-in cell line. Overexpressed mRuby2-IRSp53 concentrated at the plasma membrane and in the shaft of negative curvature tubules such as filopodia and retraction fibers but not leading edge VASP clusters.

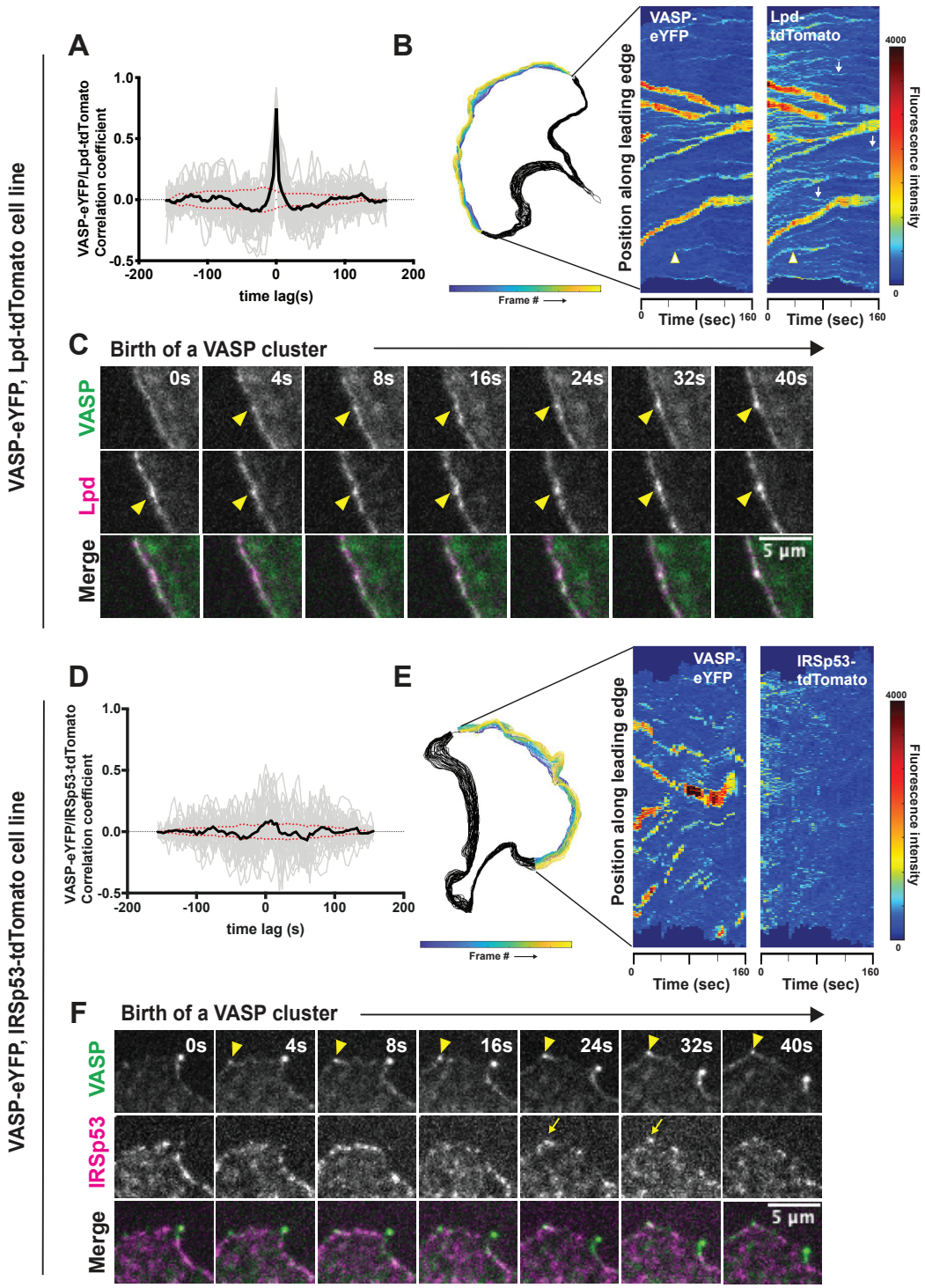

Figure 2.6: Dynamics of VASP clustering with its leading-edge binding partners, Lpd and IRSp53.

(A) Temporal cross-correlation analysis of fluctuations in VASP and Lpd intensity at leading-edge foci. Gray lines are individual cross correlation measurements and the solid black line,

which is symmetrical about zero, is the average of individual traces from 58 different clusters from four experiments. Blue dotted lines indicate an estimated 95% confidence interval of significance. Peak cross correlation occurs at time lag = 0s with a correlation coefficient of r = 0.75. (B) Cell outline of changing leading edge positions over 40 frames (left). Adaptive kymograph map (right) displaying VASP-eYFP and Lpd-tdTomato dynamics over time (40 frames; 160 seconds). (C) Frames from time-lapse microscopy of VASP clusters being born from small pre-existing Lpd clusters (arrowheads) at the leading edge in double knock-in VASP-eYFP(green)/Lpd-tdTomato (magenta) B16F1 cells. (D) Temporal cross correlation of VASP-eYFP and IRSp53-tdTomato fluorescence signal at leading edge foci. Gray lines are individual cross correlation measurements and the solid black line (the average of 34 clusters from three experiments) shows a weak peak occurring at time lag = 8s with a correlation coefficient of 0.09. Blue dotted lines indicate an estimated 95% confidence interval of significance. (E) Cell outline of changing leading edge positions over 40 frames (left). Adaptive kymograph map (right) displaying VASP-eYFP foci and IRSp53-tdTomato dynamics over time (40 frames; 160 seconds). Colormap: blue (low fluorescence intensity) to red (high fluorescence intensity). (F) Frames from time-lapse microscopy of VASP clusters (arrowhead) forming with no detectable accumulations of IRSp53-tdTomato until after the VASP foci is formed (arrow).

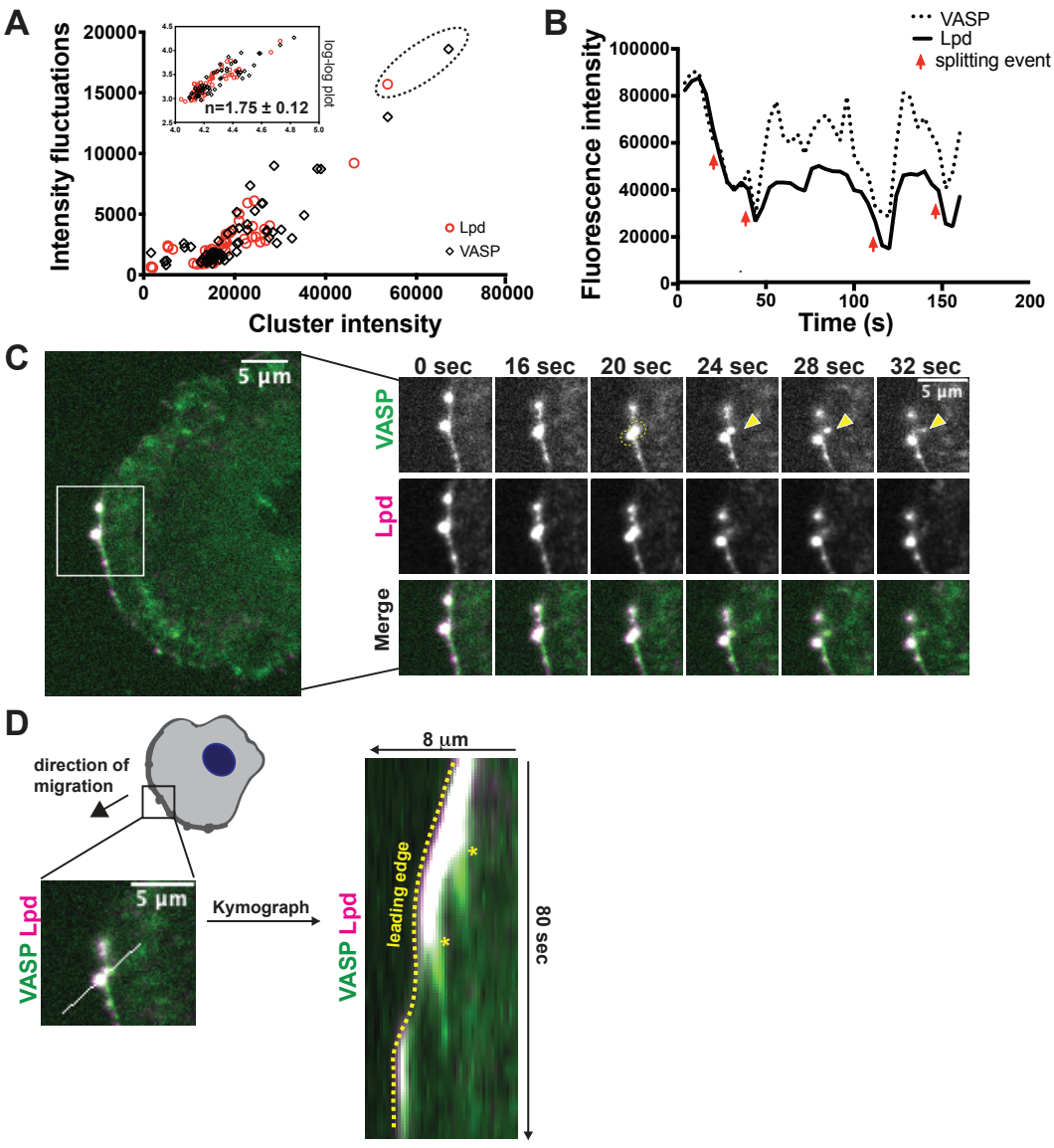

Figure 2.7: VASP/Lpd clusters exhibit size-dependent splitting behaviors.

(A) Fluctuations in VASP and Lpd were quantified by plotting the standard deviation in fluorescence intensity of VASP (black diamond) and Lpd (red circle) foci versus its time-averaged VASP (or Lpd) intensity. Inset: log plot of standard deviation vs. time-averaged VASP/Lpd intensity fits a line with slope = 1.75±0.12. (B) Intensity trace of the fluorescence intensity of a single VASP/Lpd focus from Figure 4c. Red arrows indicate simultaneous drops in both VASP and Lpd fluorescence intensity which correlate to splitting events. (C) Image (left panel) of double knock-in VASP-eYFP(green) Lpd-tdTomato(magenta) B16F1 cell with ROI indicating the VASP/Lpd cluster that undergoes a splitting event in which VASP material splits from the parental cluster (right panels, yellow arrow). (D) Kymograph of a ROI bisecting both the main VASP/Lpd cluster and secondary VASP clump that is shed indicates that the shed VASP does not move relative to the lab frame of view (asterisks). Dotted yellow line outlines the leading edge.

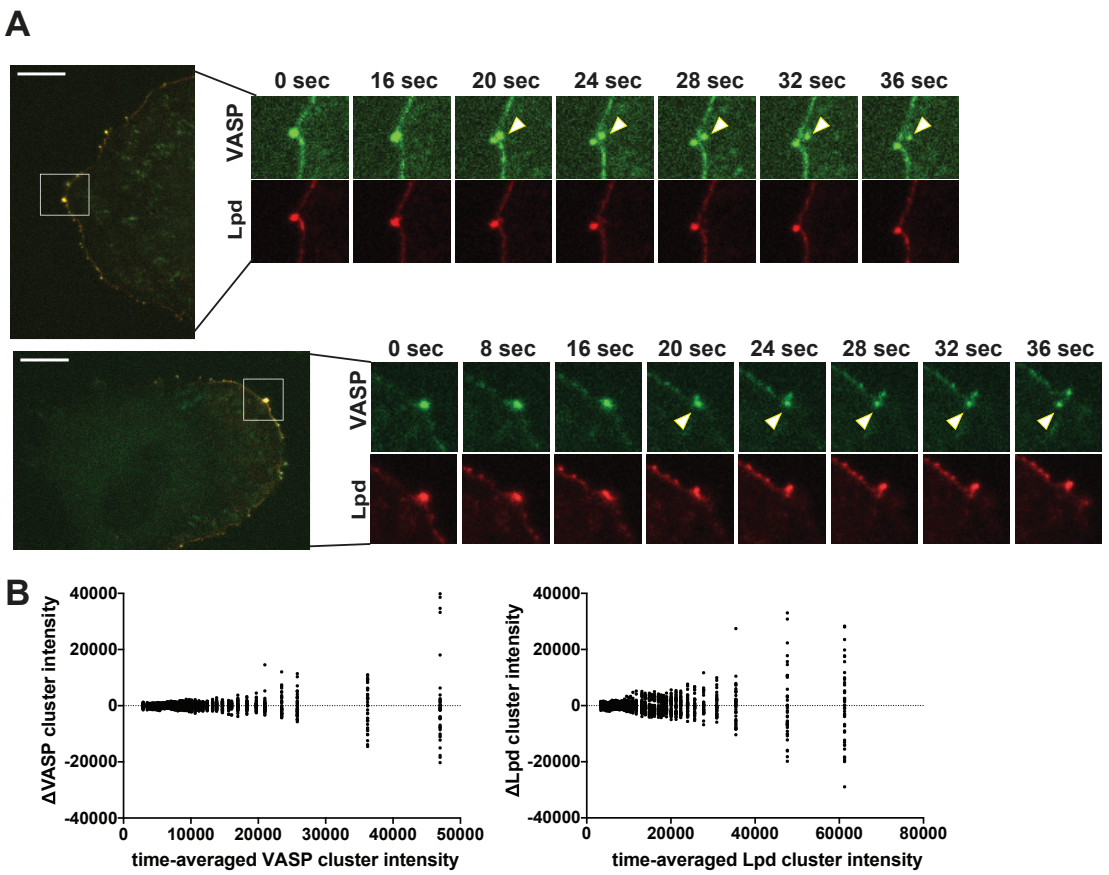

Figure 2.8: Further characterization of size-dependent splitting of VASP/Lpd clusters at the leading edge.

(A) Two additional examples of VASP/Lpd cluster splitting events. Insets represent frames capturing the splitting event with white arrowhead tracking the chunk of VASP that is left behind in the cytoplasm upon splitting. (B) Alternative visualization strategy of the size-dependency of VASP/Lpd cluster instability. The X axis represents the time-averaged cluster size over a 160 second time window given by the integrated fluorescence intensity of either VASP-eYFP (left subplot) or Lpd-tdTomato (right subplot). The Y axis represents the relative deviations of the cluster size at every time point over the 160 second imaging window (Δ cluster size = time-averaged cluster size - cluster size(t).

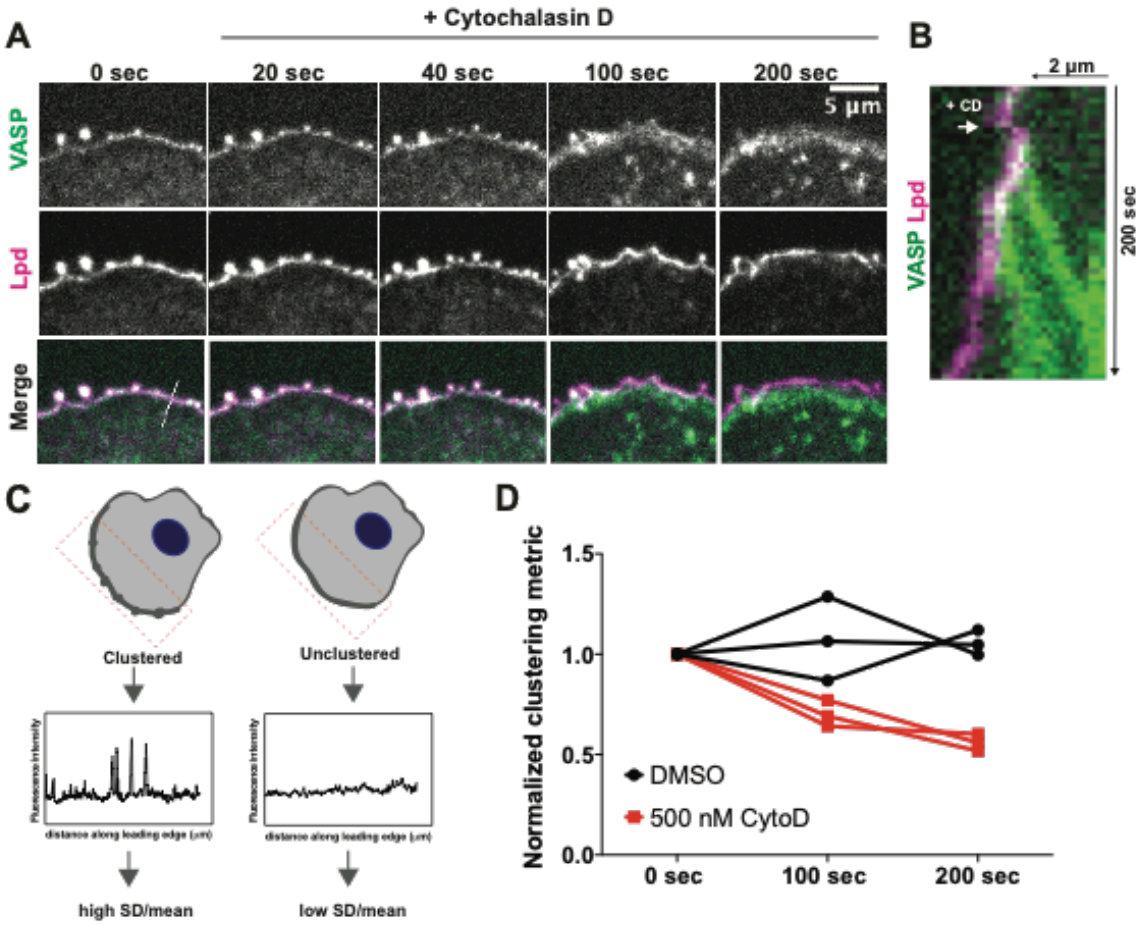

Figure 2.9: Free barbed ends of actin filaments are required for VASP/Lpd cluster stability.

(A) Representative example of a B16F1 cell expressing VASP-eYFP (green) and Lpd-tdTomato (magenta) before and after acute treatment with 500 nM Cytochalasin D. (B) Kymograph of a slice taken perpendicular to the leading edge shows change in membrane localization of VASP (green) and Lpd (magenta) upon addition of Cytochalasin D. (C) Schematic of quantification of changes in clustering. The standard deviation along a defined leading edge before (0 sec) and after drug treatment (100 sec, 200 sec) was calculated and normalized to the mean fluorescence intensity. (D) Quantification of clustering of VASP and Lpd at foci following acute treatment with Cytochalasin D or DMSO (vehicle) shows that free barbed ends are required for robust clustering of VASP and Lpd. Clustering is represented by standard deviation along the leading edge ROI before and after treatment. Symbols are averages from three biological replicates, each with >8 cells. Paired t-test of unnormalized data: p=0.02.

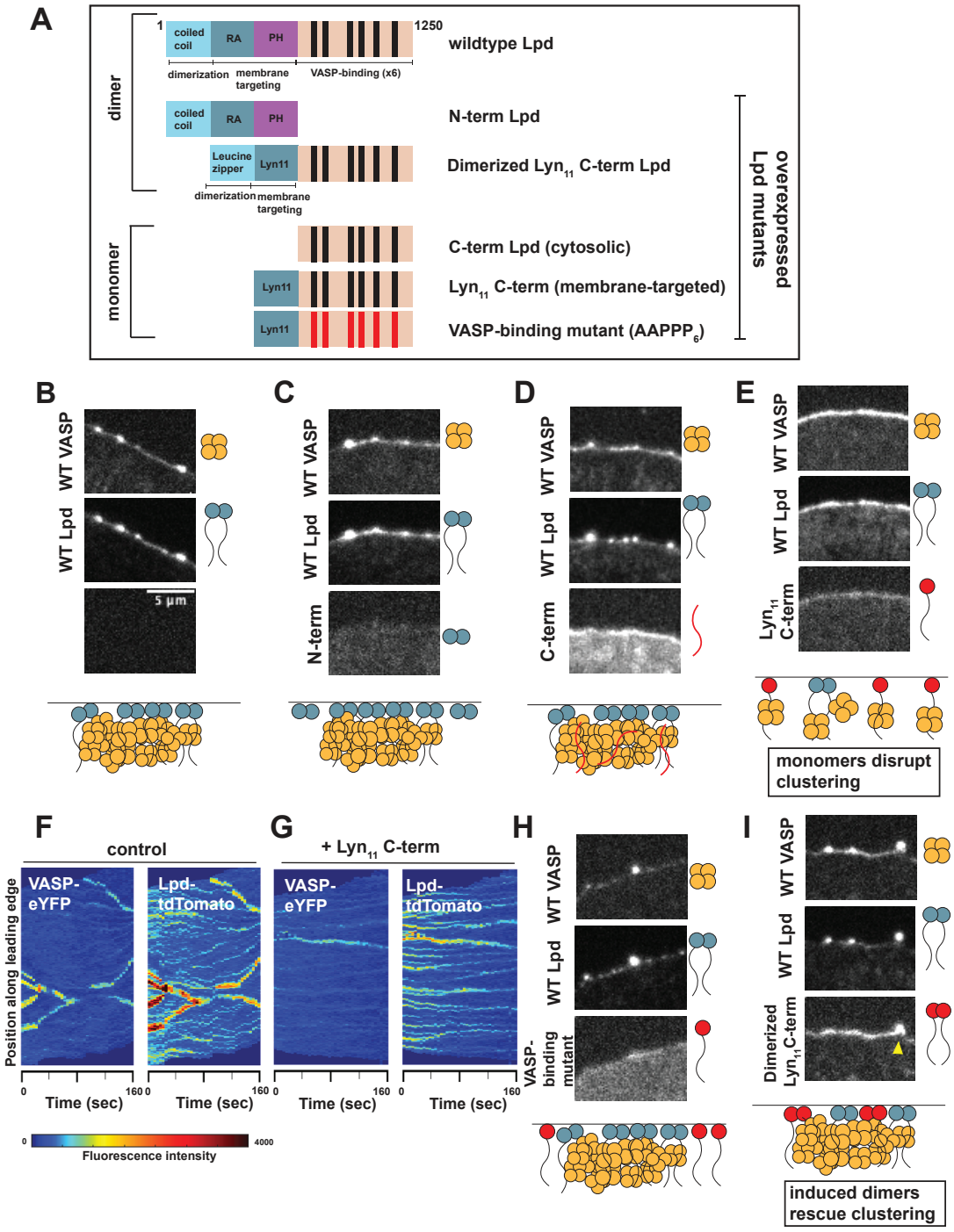

Figure 2.10: Lpd incorporation into dynamic VASP foci depends on its number of VASP binding sites.
(A) Schematic of the domain architecture of wildtype and various Lpd mutants that were overexpressed in B16F1 cells already endogenously expressing VASP-eYFP and Lpd-tdTomato. Leucine zipper (LZ) was used to orthogonally induce dimerization of the Lpd C-term; Lyn_{11} sequence was used to replace the N-term and orthogonally target C-term Lpd to the plasma membrane; VASP-binding mutant contains F/$LPPPP_6$→ $AAPPP_6$. (B-I) Representative

images from three-color microscopy of endogenous VASP-eYFP (top panel) and Lpd-tdTomato (middle panel) and various overexpressed Lpd mutants (bottom panel). All Lpd mutants were overexpressed using a CMV promoter to drive expression of the N-terminal SNAP-Lpd (labeled with Janelia Fluor 646 SNAP ligand) fusion protein. Cartoon schematic below describes the effect that overexpression of each SNAP-Lpd mutant (red) has on endogenous VASP(orange)/Lpd(blue) clustering. Yellow arrowhead: example in which dimerized Lyn_{11} C-term Lpd mutant is able to incorporate into VASP/Lpd clusters. Adaptive kymographs display leading edge VASP/Lpd clusters in (F) wild type double knock-in cells and (G) double knock-in cells with overexpressed monomeric Lyn11 C-term, which has a dominant negative effect.

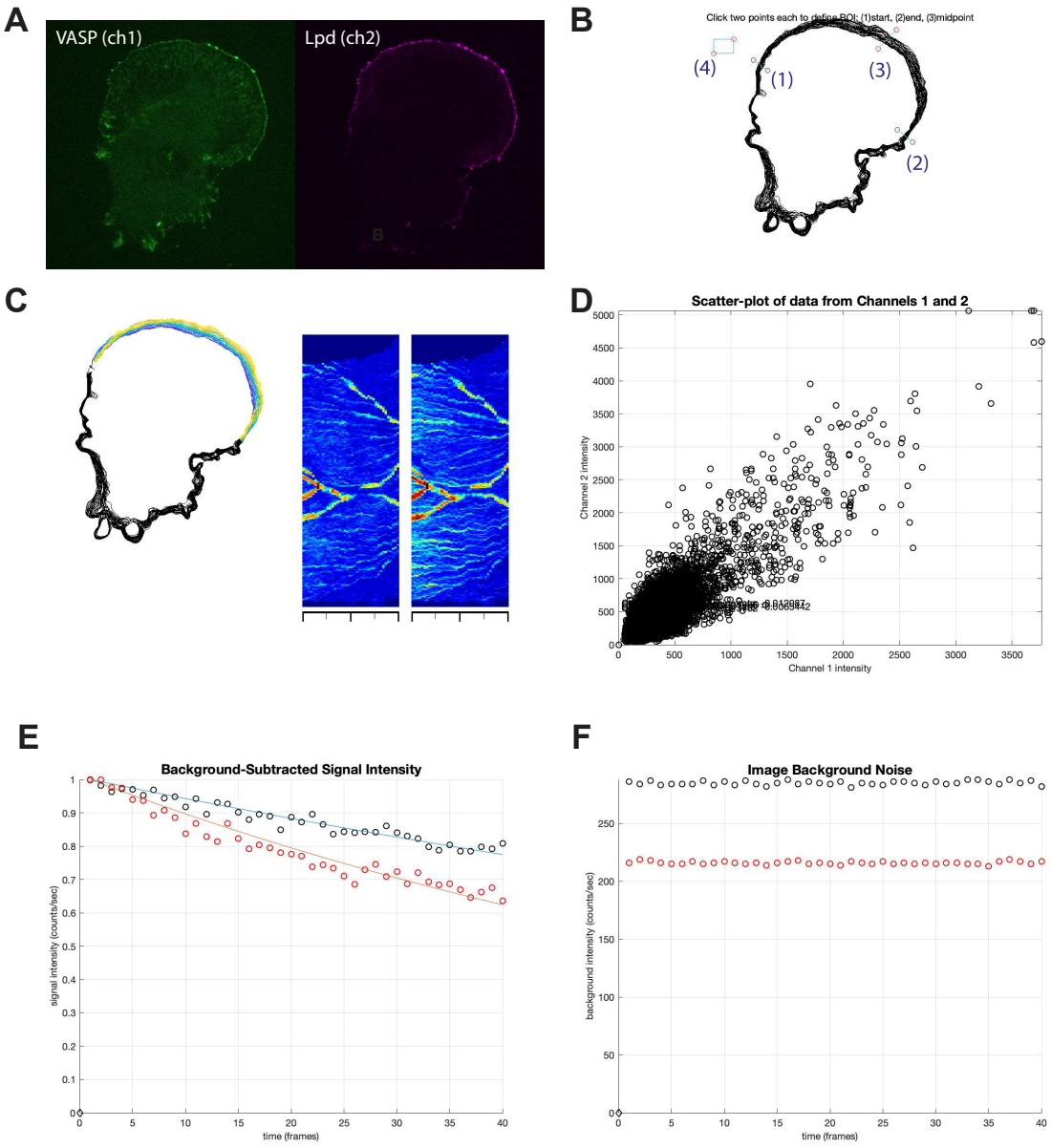

Figure 3.1: Example computational analysis inputs and outputs of dynamic cellular edges from EdgeKymograph function in Matlab.

(A) Example input is a two-color fluorescent image of leading-edge proteins VASP (left, green) and Lpd (right, magenta) from a time-lapse movie. (B) An interactive figure will pop up with the overlaid boundary lines of the cell that can be used iteratively to determine the correct parameters for the main function. (C) Example outputs include overlaid traces of the cell edge perimeter region of interest color coded by time frame (left) and adaptive kymographs of protein cluster dynamics of both VASP and Lpd channels (right). (D) An output scatterplot that displays the fluorescence of channel 1 vs. channel 2 (E) Background subtracted signal intensity used to calculate a photo-bleaching rate for VASP (red circles) and Lpd (black circles) (F) image background noise obtained from a small rectangular ROI outside of the cell collected over all the time frames.

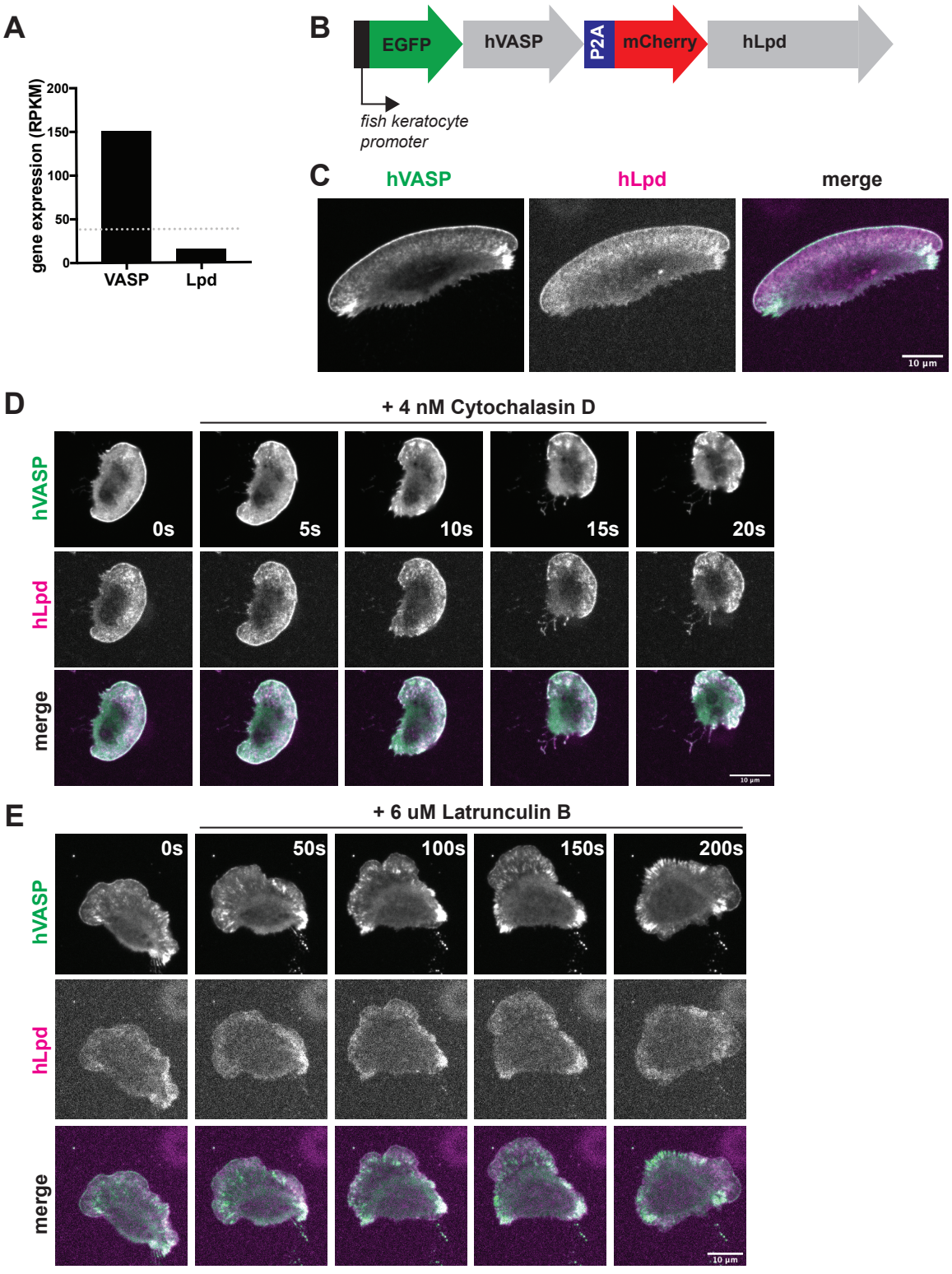

Figure 4.1: Overexpression of human VASP and lamellipodin in motile fish keratocytes.

(A) Gene expression levels of VASP and lamellipodin in zebrafish keratocytes measured by RNAseq (data from Julie Theriot lab). (B) Construct used for overexpression of human eGFP-VASP and mCherry-lamellipodin in equimolar ratios using the P2A peptide to cleave the recombinant protein in cells. (C) Representative images of migrating fish keratocytes overexpressing human eGFP-VASP and human mCherry-Lpd. (D) Representative images of migrating fish keratocytes overexpressing human eGFP-VASP and human mCherry-Lpd that have been treated with 4 nM Cytochalasin D. (E) Representative images of migrating fish keratocytes overexpressing human eGFP-VASP and human mCherry-Lpd that have been treated with 6 uM Latrunculin B.

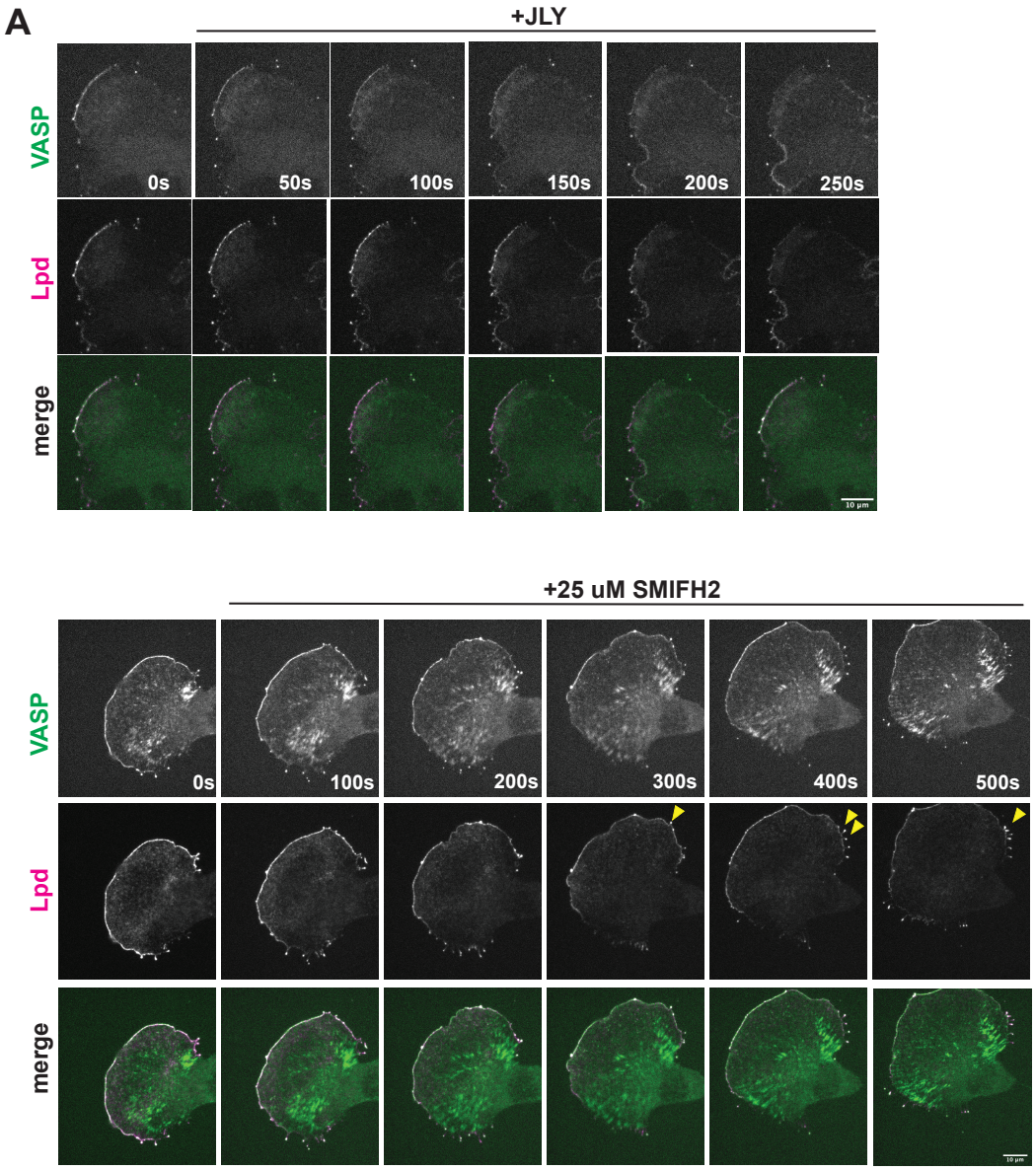

Figure 4.2: The effect of various actin inhibitors on VASP/Lpd clustering dynamics in B16F1 cells.

(A) Representative example of a B16F1 cell expressing VASP-eYFP (green) and Lpd-tdTomato (magenta) before and after acute treatment with a drug cocktail to freeze actin dynamics: 10 uM Y27632, 8 uM Jasplakinolide, and 5 uM Latrunculin B. (B) Representative example of a B16F1 cell expressing VASP-eYFP (green) and Lpd-tdTomato (magenta) before and after acute treatment with 25 uM SMIFH2, a pan-formin inhibitor.

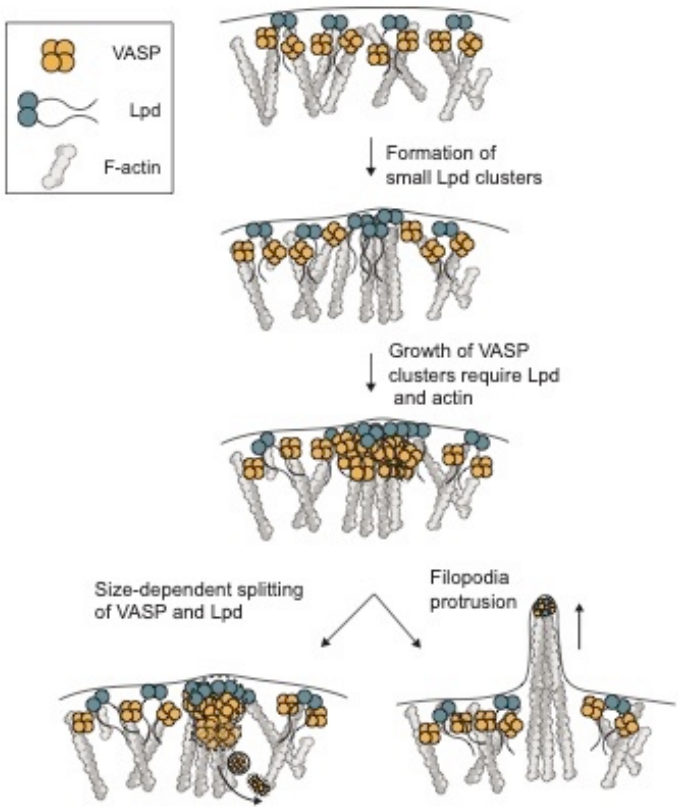

Figure 5.1: Model for clustering of VASP and lamellipodin at filopodia tip complexes.

Coalescence of VASP into leading edge clusters arises from small pre-existing lamellipodin clusters. The interaction between VASP and Lpd at clusters are mediated through multivalent interactions between EVH1 domains (VASP) and short FPPPP proline motifs (Lpd) that require membrane tethering and dimerization of Lpd. The assembly of VASP clusters involve Lpd and free barbed ends of actin filaments at the leading edge which can protrude into long filopodia or disassemble through size-dependent splitting of VASP into the cytoplasm.

Table 2.1: CRISPR/Cas9 knock-in guide sequences

Cell line generated	Parental cell line	Guide #	Guide sequence	PAM
B16F1_VASP-eYFP	B16F1	1	CCACTTGGAAGATTCCACGT	GGG
		2	CCCACTTGGAAGATTCCACG	TGG
B16F1_VASP-eYFP_Lpd-TdTomato	B16F1_VASP-eYFP	1	GGCTATGCAACATTGCGAAG	AGG
		2	CACTACCTGAATAACATATC	AGG
B16F1_VASP-eYFP_IRSp53-TdTomato	B16F1_VASP-eYFP	1	TTCAGATGGACGTTGGCGAA	GGG
		2	GGCCGATGTGAGGCGAGGCT	AGG

Table 2.2: Lamellipodin constructs used in dominant negative experiment

Plasmid name	**Construct content**
pKC117	CMV_Lyn11-SNAP-Lpd(850-1250)
pKC118	CMV_Lyn11_SNAP_Lpd(850-1250) FP6 to AP6
pKC120	CMV_Lyn11_SNAP_Lpd(850-1250) FP5 position A (AAPPP in positions B,C,D,E,F)
pKC121	CMV_Lyn11_SNAP_GGG-LZ-GGG-Lpd(850-1250)
pKC122	CMV_Lyn11-SNAP-Lpd N-term to RAPH (1-529aa)
pKC124	CMV-SNAP-Lpd(850-1250)
pKC125	CMV-SNAP-Lpd(850-1250) FP6 to AP6
pKC126	CMV-SNAP-GGG-LZ-GGG-Lpd(850-1250)
pKC136	CMV-SNAP-RAPH (1-529)
pKC138	CMV-Lyn11-SNAP-GGG-LZ-GGG-Lpd(850-1250) AP6

References

Ahmed, S., Goh, W.I. and Bu, W. 2010. I-BAR domains, IRSp53 and filopodium formation. *Seminars in Cell & Developmental Biology* 21(4), pp. 350–356.

Ball, L.J., Kühne, R., Hoffmann, B., et al. 2000. Dual epitope recognition by the VASP EVH1 domain modulates polyproline ligand specificity and binding affinity. *The EMBO Journal* 19(18), pp. 4903–4914.

Barzik, M., McClain, L.M., Gupton, S.L. and Gertler, F.B. 2014. Ena/VASP regulates mDia2-initiated filopodial length, dynamics, and function. *Molecular Biology of the Cell* 25(17), pp. 2604–2619.

Bear, J.E., Loureiro, J.J., Libova, I., Fässler, R., Wehland, J. and Gertler, F.B. 2000. Negative regulation of fibroblast motility by Ena/VASP proteins. *Cell* 101(7), pp. 717–728.

Bear, J.E., Svitkina, T.M., Krause, M., et al. 2002. Antagonism between Ena/VASP proteins and actin filament capping regulates fibroblast motility. *Cell* 109(4), pp. 509–521.

Blanchoin, L., Boujemaa-Paterski, R., Sykes, C. and Plastino, J. 2014. Actin dynamics, architecture, and mechanics in cell motility. *Physiological Reviews* 94(1), pp. 235–263.

Breitsprecher, D., Kiesewetter, A.K., Linkner, J., et al. 2008. Clustering of VASP actively drives processive, WH2 domain-mediated actin filament elongation. *The EMBO Journal* 27(22), pp. 2943–2954.

Brindle, N.P., Holt, M.R., Davies, J.E., Price, C.J. and Critchley, D.R. 1996. The focal-adhesion vasodilator-stimulated phosphoprotein (VASP) binds to the proline-rich domain in vinculin. *The Biochemical Journal* 318 (Pt 3), pp. 753–757.

Chang, Y.-C., Zhang, H., Brennan, M.L. and Wu, J. 2013. Crystal structure of Lamellipodin implicates diverse functions in actin polymerization and Ras signaling. *Protein & cell* 4(3), pp.

211–219.

Chen, X.J., Squarr, A.J., Stephan, R., et al. 2014. Ena/VASP proteins cooperate with the WAVE complex to regulate the actin cytoskeleton. *Developmental Cell* 30(5), pp. 569–584.

Coló, G.P., Lafuente, E.M. and Teixidó, J. 2012. The MRL proteins: adapting cell adhesion, migration and growth. *European Journal of Cell Biology* 91(11–12), pp. 861–868.

Damiano-Guercio, J., Kurzawa, L., Mueller, J., et al. 2020. Loss of Ena/VASP interferes with lamellipodium architecture, motility and integrin-dependent adhesion. *BioRxiv*.

Dimchev, G., Amiri, B., Humphries, A.C., et al. 2019. Lamellipodin tunes cell migration by stabilizing protrusions and promoting adhesion formation. *BioRxiv*.

Disanza, A., Bisi, S., Winterhoff, M., et al. 2013. CDC42 switches IRSp53 from inhibition of actin growth to elongation by clustering of VASP. *The EMBO Journal* 32(20), pp. 2735–2750.

Fritz-Laylin, L.K., Riel-Mehan, M., Chen, B.-C., et al. 2017. Actin-based protrusions of migrating neutrophils are intrinsically lamellar and facilitate direction changes. *eLife* 6.

Gertler, F.B., Niebuhr, K., Reinhard, M., Wehland, J. and Soriano, P. 1996. Mena, a relative of VASP and Drosophila Enabled, is implicated in the control of microfilament dynamics. *Cell* 87(2), pp. 227–239.

Hansen, S.D. and Mullins, R.D. 2015. Lamellipodin promotes actin assembly by clustering Ena/VASP proteins and tethering them to actin filaments. *eLife* 4.

Hansen, S.D. and Mullins, R.D. 2010. VASP is a processive actin polymerase that requires monomeric actin for barbed end association. *The Journal of Cell Biology* 191(3), pp. 571–584.

Han, Y.-H., Chung, C.Y., Wessels, D., et al. 2002. Requirement of a vasodilator-stimulated phosphoprotein family member for cell adhesion, the formation of filopodia, and chemotaxis in dictyostelium. *The Journal of Biological Chemistry* 277(51), pp. 49877–49887.

Korobova, F. and Svitkina, T. 2008. Arp2/3 complex is important for filopodia formation, growth cone motility, and neuritogenesis in neuronal cells. *Molecular Biology of the Cell* 19(4), pp. 1561–1574.

Krause, M., Leslie, J.D., Stewart, M., et al. 2004. Lamellipodin, an Ena/VASP ligand, is implicated in the regulation of lamellipodial dynamics. *Developmental Cell* 7(4), pp. 571–583.

Krugmann, S., Jordens, I., Gevaert, K., Driessens, M., Vandekerckhove, J. and Hall, A. 2001. Cdc42 induces filopodia by promoting the formation of an IRSp53:Mena complex. *Current Biology* 11(21), pp. 1645–1655.

Kwiatkowski, A.V., Rubinson, D.A., Dent, E.W., et al. 2007. Ena/VASP Is Required for neuritogenesis in the developing cortex. *Neuron* 56(3), pp. 441–455.

Lacayo, C.I., Pincus, Z., VanDuijn, M.M., et al. 2007. Emergence of large-scale cell morphology and movement from local actin filament growth dynamics. *PLoS Biology* 5(9), p. e233.

Lafuente, E.M., van Puijenbroek, A.A.F.L., Krause, M., et al. 2004. RIAM, an Ena/VASP and Profilin ligand, interacts with Rap1-GTP and mediates Rap1-induced adhesion. *Developmental Cell* 7(4), pp. 585–595.

Lewis, A.K. and Bridgman, P.C. 1992. Nerve growth cone lamellipodia contain two populations of actin filaments that differ in organization and polarity. *The Journal of Cell Biology* 119(5), pp. 1219–1243.

Lim, K.B., Bu, W., Goh, W.I., et al. 2008. The Cdc42 effector IRSp53 generates filopodia by coupling membrane protrusion with actin dynamics. *The Journal of Biological Chemistry* 283(29), pp. 20454–20472.

Mattila, P.K. and Lappalainen, P. 2008. Filopodia: molecular architecture and cellular functions. *Nature Reviews. Molecular Cell Biology* 9(6), pp. 446–454.

Mattila, P.K., Pykäläinen, A., Saarikangas, J., et al. 2007. Missing-in-metastasis and IRSp53 deform PI(4,5)P2-rich membranes by an inverse BAR domain-like mechanism. *The Journal of Cell Biology* 176(7), pp. 953–964.

Mejillano, M.R., Kojima, S., Applewhite, D.A., Gertler, F.B., Svitkina, T.M. and Borisy, G.G. 2004. Lamellipodial versus filopodial mode of the actin nanomachinery: pivotal role of the filament barbed end. *Cell* 118(3), pp. 363–373.

Millard, T.H., Bompard, G., Heung, M.Y., et al. 2005. Structural basis of filopodia formation induced by the IRSp53/MIM homology domain of human IRSp53. *The EMBO Journal* 24(2), pp. 240–250.

Mogilner, A. and Rubinstein, B. 2005. The physics of filopodial protrusion. *Biophysical Journal* 89(2), pp. 782–795.

Nakagawa, H., Miki, H., Nozumi, M., et al. 2003. IRSp53 is colocalised with WAVE2 at the tips of protruding lamellipodia and filopodia independently of Mena. *Journal of Cell Science* 116(Pt 12), pp. 2577–2583.

Niebuhr, K., Ebel, F., Frank, R., et al. 1997. A novel proline-rich motif present in ActA of Listeria monocytogenes and cytoskeletal proteins is the ligand for the EVH1 domain, a protein module present in the Ena/VASP family. *The EMBO Journal* 16(17), pp. 5433–5444.

Oldenbourg, R., Katoh, K. and Danuser, G. 2000. Mechanism of lateral movement of filopodia and radial actin bundles across neuronal growth cones. *Biophysical Journal* 78(3), pp. 1176–1182.

Prehoda, K.E., Lee, D.J. and Lim, W.A. 1999. Structure of the enabled/vasp homology 1 domain–peptide complex. *Cell* 97(4), pp. 471–480.

Prévost, C., Zhao, H., Manzi, J., et al. 2015. IRSp53 senses negative membrane curvature and phase separates along membrane tubules. *Nature Communications* 6, p. 8529.

Ran, F.A., Hsu, P.D., Wright, J., Agarwala, V., Scott, D.A. and Zhang, F. 2013. Genome engineering using the CRISPR-Cas9 system. *Nature Protocols* 8(11), pp. 2281–2308.

Reinhard, M., Halbrügge, M., Scheer, U., Wiegand, C., Jockusch, B.M. and Walter, U. 1992. The 46/50 kDa phosphoprotein VASP purified from human platelets is a novel protein associated with actin filaments and focal contacts. *The EMBO Journal* 11(6), pp. 2063–2070.

Reinhard, M., Rüdiger, M., Jockusch, B.M. and Walter, U. 1996. VASP interaction with vinculin: a recurring theme of interactions with proline-rich motifs. *FEBS Letters* 399(1–2), pp. 103–107.

Rottner, K., Behrendt, B., Small, J.V. and Wehland, J. 1999. VASP dynamics during lamellipodia protrusion. *Nature Cell Biology* 1(5), pp. 321–322.

Saarikangas, J., Zhao, H., Pykäläinen, A., et al. 2009. Molecular mechanisms of membrane deformation by I-BAR domain proteins. *Current Biology* 19(2), pp. 95–107.

Schmeiser, C. and Winkler, C. 2015. The flatness of Lamellipodia explained by the interaction between actin dynamics and membrane deformation. *Journal of Theoretical Biology* 380, pp. 144–155.

Sudhaharan, T., Hariharan, S., Lim, J.S.Y., et al. 2019. Superresolution microscopy reveals distinct localisation of full length IRSp53 and its I-BAR domain protein within filopodia. *Scientific Reports* 9(1), p. 2524.

Svitkina, T.M., Bulanova, E.A., Chaga, O.Y., et al. 2003. Mechanism of filopodia initiation by reorganization of a dendritic network. *The Journal of Cell Biology* 160(3), pp. 409–421.

Vignjevic, D., Yarar, D., Welch, M.D., Peloquin, J., Svitkina, T. and Borisy, G.G. 2003. Formation of filopodia-like bundles in vitro from a dendritic network. *The Journal of Cell Biology* 160(6), pp. 951–962.

Weiner, O.D., Marganski, W.A., Wu, L.F., Altschuler, S.J. and Kirschner, M.W. 2007. An actin-

based wave generator organizes cell motility. *PLoS Biology* 5(9), p. e221.

Welch, M.D. and Mullins, R.D. 2002. Cellular control of actin nucleation. *Annual Review of Cell and Developmental Biology* 18, pp. 247–288.

Yamagishi, A., Masuda, M., Ohki, T., Onishi, H. and Mochizuki, N. 2004. A novel actin bundling/filopodium-forming domain conserved in insulin receptor tyrosine kinase substrate p53 and missing in metastasis protein. *The Journal of Biological Chemistry* 279(15), pp. 14929–14936.

Yang, C., Hoelzle, M., Disanza, A., Scita, G. and Svitkina, T. 2009. Coordination of membrane and actin cytoskeleton dynamics during filopodia protrusion. *Plos One* 4(5), p. e5678.

Yang, C. and Svitkina, T. 2011. Filopodia initiation: focus on the Arp2/3 complex and formins. *Cell Adhesion & Migration* 5(5), pp. 402–408.

Young, L.E., Heimsath, E.G. and Higgs, H.N. 2015. Cell type-dependent mechanisms for formin-mediated assembly of filopodia. *Molecular Biology of the Cell* 26(25), pp. 4646–4659.

Young, L.E., Latario, C.J. and Higgs, H.N. 2018. Roles for Ena/VASP proteins in FMNL3-mediated filopodial assembly. *Journal of Cell Science* 131(21).

Zoubir, A.M. and Iskander, D.R. 2004. *Bootstrap techniques for signal processing*. Cambridge: Cambridge University Press.

Publishing Agreement

It is the policy of the University to encourage open access and broad distribution of all theses, dissertations, and manuscripts. The Graduate Division will facilitate the distribution of UCSF theses, dissertations, and manuscripts to the UCSF Library for open access and distribution. UCSF will make such theses, dissertations, and manuscripts accessible to the public and will take reasonable steps to preserve these works in perpetuity.

I hereby grant the non-exclusive, perpetual right to The Regents of the University of California to reproduce, publicly display, distribute, preserve, and publish copies of my thesis, dissertation, or manuscript in any form or media, now existing or later derived, including access online for teaching, research, and public service purposes.

DocuSigned by:
Karen Cheng
339398FD38AA47F...
Author Signature

9/4/2020
Date